The effect of streamwise braid vortices on the particle dispersion in a plane mixing layer. II. Nonlinear particle dynamics

B. Marcu, E. Meiburg,[a] and N. Raju
Department of Aerospace Engineering, University of Southern California, Los Angeles, California 90089-1191

(Received 8 June 1995; accepted 25 October 1995)

A computational investigation of the nonlinear dynamics of heavy particles in a row of counterrotating strained vortices is presented. By tracking the particles numerically in the quasi-two-dimensional fluid velocity field, information is obtained on the nature of their trajectories, as well as on probability distribution functions and potential accumulation regions. The particle behavior is discussed as a function of the dimensionless strain rate, the particle Stokes number St, and the dimensionless gravity parameter Fr. Only for very low values of the St can the particles accumulate at the vortex centers. For moderate values of St, they remain trapped on closed trajectories around the vortex centers. Increasing St leads to periodic open trajectories that allow for spanwise transport of the particles. Further bifurcations lead to the generation of multiple trajectories, as well as to subharmonic solutions. Eventually, intermittent and chaotic particle dynamics are observed. In the chaotic regime, a simplified flow model is employed in order to derive various scaling laws for the particle concentration field. For strong levels of gravity, the accumulation of large numbers of particles is observed in the upwelling regions predicted in part I of the present investigation [B. Marcu and E. Meiburg, Phys. Fluids **8**, 715 (1996)]. © *1996 American Institute of Physics.* [S1070-6631(96)00403-3]

I. INTRODUCTION

In Part I of the present investigation,[1] we introduced an analytical model of the counterrotating strained streamwise braid vortices commonly found in three-dimensionally developing plane mixing layers.[2–6] These flow structures are expected to result in a significant modification of the dominant two-dimensional particle dispersion mechanisms,[7–12] which are known to lead to the formation of bands of particles in the braid region. We investigated analytically the circumstances under which heavy particles can be trapped at the centers of the strained vortex structures, and whether or not these vortices can lead to an accumulation of particles in certain regions of the flow field. One of the main findings was that, in the absence of gravity, only particles below a critical value of the Stokes number St_{crit} can be trapped at the vortex centers. For larger values of St, the vortices' tendency to eject heavy particles overcomes the strain's ability to trap them, so that accumulation at the vortex centers is not possible. However, in the presence of gravity multiple equilibrium points with different stability characteristics can exist. In particular, for a horizontal mixing layer and strong gravitational effects, unconditional accumulation can occur in the upwelling regions midway between the streamwise braid vortices.

While in Part I, we addressed the existence and linear stability of equilibrium points in an array of counterrotating streamwise vortices, we will now focus on the nonlinear dynamics of heavy particles in such flows. In particular, it is of interest to obtain information regarding the size of the basin of attraction of stable equilibrium points, as well as about the nonlinear particle dynamics and related concentration fields should stable equilibrium points not exist. We address these issues by means of numerical simulations of the nonlinear particle dynamics for a variety of different conditions. The nature of these simulations will be described in Section II. The calculations exhibit a rich dynamical behavior of the particles, with qualitative differences for low, intermediate, and high strain intensities. In Section III we will describe these results in the absence of gravity, while in Section IV we will address the ways in which gravity modifies the particle dynamics. Dispersion of heavy particles in the fully chaotic regime will be analyzed in Section V, along with gravity effects on the particle dispersion field, and a description of the particle accumulation process. In Section VI we will present some conclusions from the present investigation.

II. NUMERICAL SIMULATIONS

The present investigation of particle dispersion in the braid region of a plane mixing layer (Fig. 1) is based on the analytical flow model developed by Marcu and Meiburg.[1] The non-dimensional fluid velocity field (w_f, v_f) in the cross-stream z,y-plane is expressed by the relationships

$$w_f = -0.5\frac{\sinh[2\pi(y-y_0)]}{\cosh[2\pi(y-y_0)]-k\cos[2\pi(z-z_0)]} + 0.5\frac{\sinh[2\pi(y-y_1)]}{\cosh[2\pi(y-y_1)]-k\cos[2\pi(z-z_1)]}, \quad (1)$$

[a]Corresponding author: Department of Aerospace Engineering, University of Southern California, Los Angeles, California 90089-1191. Phone: 213-740-5376; fax: 213-740-7774.

 1070-6631/96/8(3)/734/20/$10.00

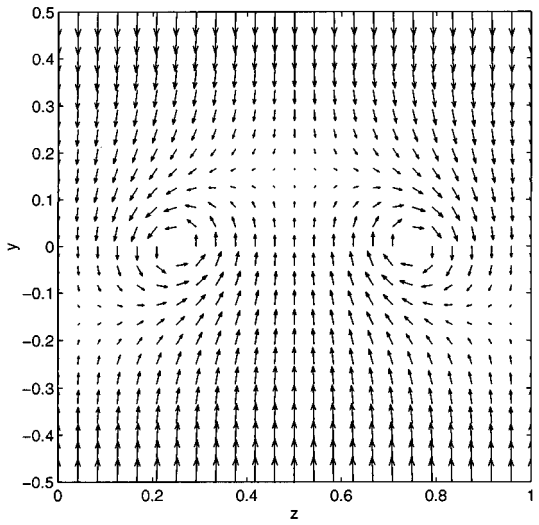

FIG. 1. Fluid velocity field for the row of counterrotating vortices in the cross-stream, (z,y)-plane for $\sigma=4.0$ and $k=0.9$.

$$v_f = 0.5\,\frac{k\sin[2\pi(z-z_0)]}{\cosh[2\pi(y-y_0)]-k\cos[2\pi(z-z_0)]} - 0.5\,\frac{k\sin[2\pi(z-z_1)]}{\cosh[2\pi(y-y_1)]-k\cos[2\pi(z-z_1)]} - \sigma y. \tag{2}$$

Here, (z_0,y_0) and (z_1,y_1) denote the locations of the vortex centers, which we place at (0.25,0) and (0.75,0). The flow is periodic in the spanwise z-direction, with a period equal to the unit width of the computational domain. The velocity $\mathbf{V}_p=(w_p,v_p)$ and location $\mathbf{x}_p$ of a small spherical particle of diameter d in the fluid velocity field $\mathbf{U}=(w_f,v_f)$ are then governed by the dimensionless equations[13]

$$\frac{d\mathbf{V}_p}{dt}=\frac{1}{St}(\mathbf{U}|_{\mathbf{x}=\mathbf{x}_p}-\mathbf{V}_p)+\frac{1}{Fr^2}\mathbf{e_g}, \tag{3}$$

$$\frac{d\mathbf{x}_p}{dt}=\mathbf{V}_p. \tag{4}$$

Here $\mathbf{e}_g$ represents the unit vector in the direction of the projection of gravity on the z,y-plane. Lengths, time, and velocities were rendered dimensionless by the characteristic velocity ΔW, which is related to the strength of the streamwise vortices,[1] and by the spanwise wavelength λ_z of the row of counterrotating streamwise vortices. The dimensionless parameters

$$St=\frac{d^2\rho_p\Delta W}{18\rho_f\nu_f\lambda_z} \tag{5}$$

and

$$Fr=\frac{\Delta W}{\sqrt{\lambda_z g}}, \tag{6}$$

are the Stokes and Froude numbers, respectively. Here ν_f denotes the kinematic viscosity of the fluid and g represents the length of the projection of gravity on the z,y-plane. Notice that, as a result of the above scaling, the Stokes number St of a particle will vary as the characteristic velocity describing the strength of the streamwise vortices ΔW or their spatial spacing λ_z change during the evolution of the flow field. As is well known, St indicates the ratio of the particle's aerodynamic response time and the characteristic fluid flow time scale, while Fr expresses in dimensionless form the relative importance of inertial and gravitational forces. As Fr decreases, gravity becomes more important for the dynamical behavior of the particle. As in Part I of this investigation,[1] we only consider the effects of inertia, drag, and gravity. Consequently, the results can be expected to hold in the limit of large particle to fluid density ratios. The order of magnitude analysis conducted by Lazaro and Lasheras[8] indicates that in this limit the effects of flow nonuniformity, virtual mass, Basset history force, and Saffman lift force are negligible. In order to investigate the influence of higher order effects, we took into account a nonlinear drag law in our earlier study of two-dimensional mixing layers.[12] We found that the particle dynamics do not change qualitatively, but that they may be shifted to slightly different values of St. We assume the same would hold true in the present case if we included the above higher order effects in our simulations.

Equations (3) and (4) are written as a nonlinear four-dimensional system for z_p, y_p, w_p, and v_p,[1,14,15] yielding

$$\dot{\mathbf{x}}=\mathbf{F}(x), \tag{7}$$

where

$$\mathbf{x}=\begin{bmatrix} z_p \\ y_p \\ w_p \\ v_p \end{bmatrix}, \qquad \mathbf{F}(x)=\begin{bmatrix} w_p \\ v_p \\ \dfrac{1}{St}(w_f-w_p)+\dfrac{e_{gz}}{Fr^2} \\ \dfrac{1}{St}(v_f-v_p)+\dfrac{e_{gy}}{Fr^2} \end{bmatrix}. \tag{8}$$

Here e_{gz} and e_{gy} represent the z- and y-components of the unit vector in the direction of the z,y-projection of the gravity vector. This system of ordinary differential equations, with appropriate initial conditions specified for $t=0$, constitutes a nonlinear dissipative dynamical system. We advance the system of equations (7) and (8) in time by a standard fourth order Runge-Kutta method. In order to obtain detailed information on the short-time and long-time aspects of the particle motion, three different types of simulations are performed:

During the initial stages of the investigation, the motion of 10,000 particles was computed simultaneously for moderately long time periods, and for a variety of different combinations of k, σ, St, and Fr. The particles were seeded randomly over the whole or upper half of the computational box, with their initial velocities equal to the local fluid velocity. Subsequently, they were tracked in time, and their instantaneous positions recorded at different time levels. Snapshots of the particle distributions at different times demonstrate their tendency towards accumulation along specific attractors or in certain regions. The large number of particles in each simulation maximizes the probability that all existing and stable attractors will be identified.

During the following stages, small sets of 10 to 50 particles were simultaneously tracked for longer times, in order to analyze the long-time behavior of the particles in more detail.

In order to analyze changes in the attractors, i.e., in the particle trajectories, as a function of the dimensionless parameters, simulations using only one particle were carried out. The initial position of the particle, along the line $y=0$, was found after several tests, such that the particular desired trajectory could be captured. Then, repeated one-particle simulations using constant initial conditions, and varying one of the particle parameters St or Fr, enabled us to study the particular effects of particle inertia and gravity on the nature and form of the trajectory.

Details of the computational procedures used to obtain statistical data are provided in Section V.

Repeated simulations were conducted to test the accuracy, and to choose the time step size. Since the particle parameters St and Fr were varied over a large range of values, the time step was also varied, in order to ensure the accuracy of the simulation. The range of time step values was $0.001 \leqslant \Delta t \leqslant 0.05$. Small time steps were used for small St values, and for strong gravity cases corresponding to small Fr values. The validity of the results was checked by repeating the simulation with the time step size cut in half. In particular, observations of bifurcations, as well as computations of Poincaŕe sections were verified using a very small time step of $\Delta t=0.001$. The asymptotic accumulation of particles along certain trajectories was tested by extending the simulations to fivefold longer times.

III. LONG TERM DYNAMICAL BEHAVIOR OF PARTICLES IN THE ABSENCE OF GRAVITY

As a first step, we investigate the solutions for particle trajectories in the absence of gravity, focusing on the balance between the viscous and inertial forces on the particle. Inertial properties, expressed by the Stokes number St, alter the trajectory of the particle from that of a fluid marker by continuously generating a phase shift between the particle motion and the forcing fluid velocity field.

Corcos and Sherman[16] derive the scaling law for the dimensional strain parameter $\tilde{\sigma}$,

$$\tilde{\sigma}=\frac{3\Delta U}{\lambda_x}, \tag{9}$$

where ΔU is the velocity difference between the upper and the lower layer streams of the mixing layer, and λ_x is the spacing between the Kelvin-Helmholtz rollers. By combining this relationship with the experimental observation by Bernal and Roshko[2] that the spacing between the streamwise vortices $\lambda_z \approx \frac{2}{3}\lambda_x$, Marcu and Meiburg[1] showed that the non-dimensional strain parameter σ can only take values above the minimum of $\sigma \simeq 2$, which corresponds to fully developed, strong streamwise vortices. A typical value for the early stages of the streamwise vortices' growth can be given based on the experimental results of Bell and Mehta.[4] Here their measurements show the circulation of the streamwise vortices to be approximately ten per cent of that of the spanwise rollers. Using the scaling analysis by Marcu and Meiburg,[1] a value of $\sigma \simeq 13$ is obtained for the non-dimensional strain factor.

A typical, moderate dimensionless strain value is based on the situation when the streamwise vortices reach half of the spanwise vortices' strength. The value corresponding to this case is $\sigma \simeq 4$.

A. Particle behavior at moderate strain

Here the flow parameters are $k=0.9$ and $\sigma=4.0$. Under these conditions, the critical St value for particle accumulation[1] is

$$St_{cr}=\frac{2\sigma}{4[2\pi k/(1-k^2)]^2-\sigma^2}=0.0023.$$

Only below this critical value, accumulation at the center of the vortex is possible. This critical value of St was confirmed numerically by carrying out simulations for slightly smaller and slightly larger values of St, respectively. For larger, but still moderate values of St, Figs. 2(a)–(c) show the instantaneous positions of 10,000 particles initially randomly seeded in the upper half of the computational box, with initial velocities equal to the fluid velocity. The computations are run for a period of time long enough to allow for the particles to approach their asymptotic and stable trajectory. All of the randomly seeded particles characterized by $St=0.2$ collect along closed trajectories around the vortices, as shown in Fig. 2(a). These closed particle trajectories are due to a balance between viscous drag and inertial forces only, as opposed to those observed in previous studies[14,15] applicable to the main co-rotating spanwise vortices, where the centrifugal forces were balanced by the pressure forces in the flow field around the vortices. In the present case, the closed orbits are characterized by the balance between the centrifugal (inertial) forces, which tend to eject the particles out of the vortex cores, and the viscous drag force caused by the strain, which brings the particles back to the vortex row. This situation is similar to the dynamics of heavy particles in a Burgers vortex,[17] where they collect along circular trajectories around the vortex center.[18]

As the inertial forces become more important, a tendency of the particles to break-up the closed loop trajectory becomes evident by small overshoots at the corners of the loops, as shown in Fig. 2(b) for $St=0.23$. The overshoots become longer as St increases, until they touch the neighboring trajectory, which has an opposite sense of rotation. At a critical value of St, the closed loops open, and a spatially periodic solution emerges. The spatial period is unity, which is equal to that of the fluid velocity field. Figure 2(c) shows the instantaneous particle positions for $St=0.30$. All of the particles collect along the period one solution, which has two symmetric branches, allowing for particle transport either to the left or to the right of the computational box. Notice the symmetry of each of the two branches with respect to the sections above and below $y=0$. This symmetry is expressed by the fact that if the section above $y=0$ of a branch is

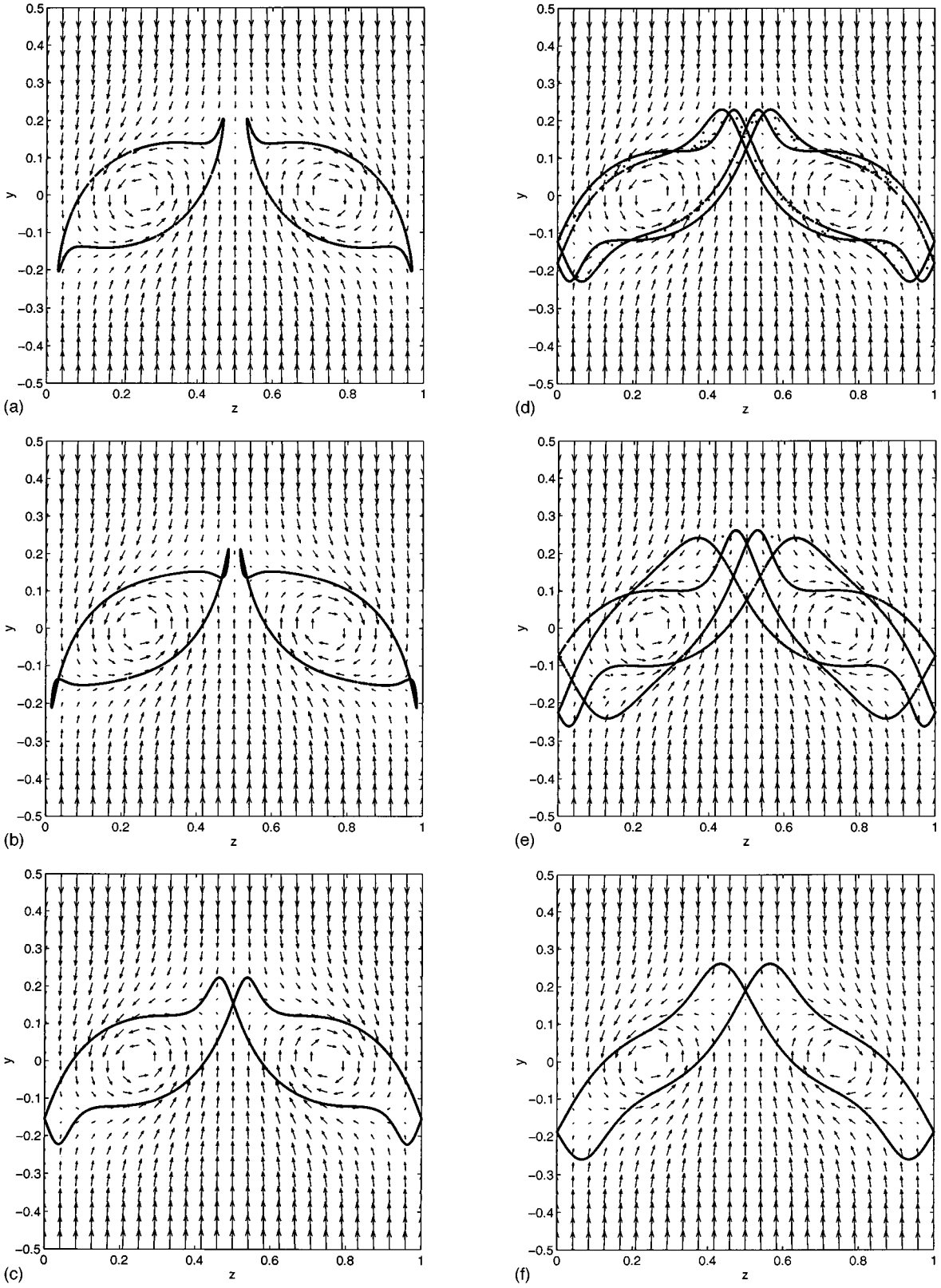

FIG. 2. Particle trajectories in the absence of gravity, $k=0.9$; $\sigma=4.0$. (a) $St=0.20$. Particle collect along closed loop trajectories around each vortex. (b) $St=0.23$. Increased inertia generates small overshoots at the corners of the loops preceding their break-up. (c) $St=0.30$. Particles collect along open periodic trajectories with a spatial period equal to unity. (d) $St=0.40$. A symmetry breaking bifurcation leads to a second stable particle trajectory. (e) $St=0.56$. The two trajectories are distinct, with different amplitudes. (f) $St=0.67$. Unique basic solution for the particle trajectory. The two trajectories have merged into a single, stable one (g) $St=0.78$. A bifurcation allows for two different types of solutions for particle trajectories: a basic solution (period unity) and a subharmonic solution with spatial period equal to three. (h) $St=0.93$. Basic solution only. The two different trajectories have again marged into a unique stable one. (i) $St=0.95$. Again , a bifurcation allows for the existence of two different solutions for particle trajectaories: a basic solution (period unity) and a subharmonic solution with spatial period equal to two.

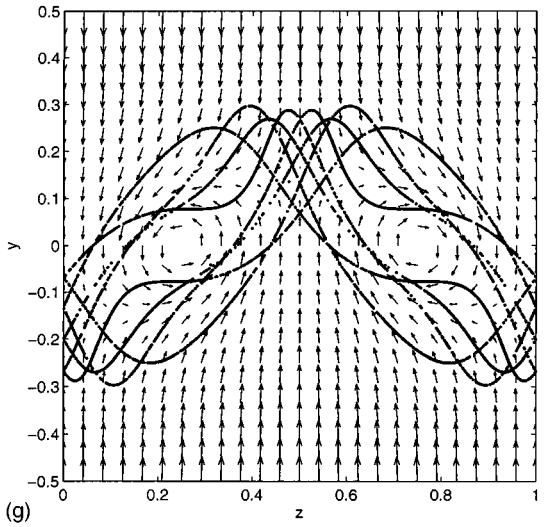

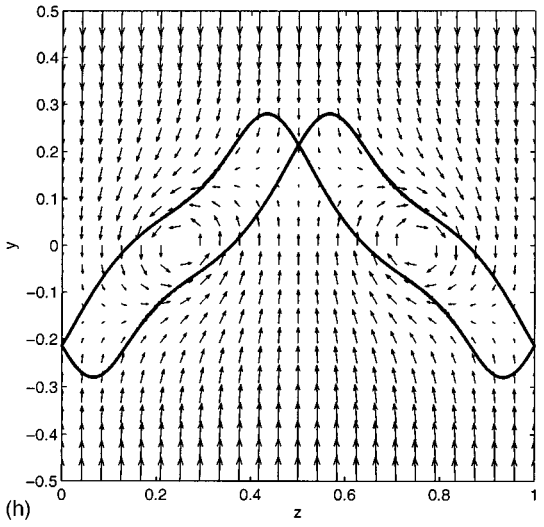

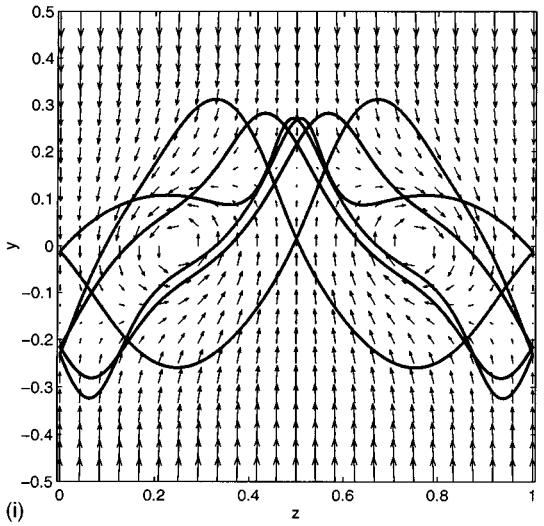

FIG. 2. (*Continued.*)

flipped below $y=0$ and shifted by one half unit in the z-direction, it will be identical to the section of the branch below $y=0$.

In the following discussion, we consider the two symmetric branches of a period unity particle trajectory to be part of the same *basic solution.* Physically, this solution demonstrates that, in spite of the symmetries of the fluid velocity field, the particle's inertia enables it to regularly escape from each vortex by oscillating in the vertical direction, and thereby to continue to travel along its periodic path in the spanwise direction. In other words, the particle's inertia allows it to break the symmetry of the fluid velocity field, thereby enabling spanwise particle transport in the plane mixing layer.

As we increase St further, we observe a series of bifurcations of the above basic solution, cf. Figs. 2(d)–(i). These bifurcations can lead to the emergence of multiple stable period one trajectories, or to the appearance of subharmonic trajectories through period doubling. For $St=0.40$, a second, stable solution appears as a result of a symmetry-breaking bifurcation, as shown in Fig. 2(d). Now the sections above $y=0$ of a solution are no longer symmetric to those sections below $y=0$ of the same solution. However, through flipping and shifting, the two trajectories along which the particles travel in the same direction can still be shown to have identical shapes. As St is further increased, the asymmetry of the $y>0$ and the $y<0$ sections of the same solution becomes more pronounced, cf. Fig. 2(e) for $St=0.56$. When we increase St further to 0.67, the trajectories merge, and the $y>0$ and $y<0$ sections of the same trajectory have become symmetric once again, cf. Fig. 2(f).

As we further increase St, subsequent bifurcations of different kinds produce a variety of secondary solutions. Figure 2(g) shows particle trajectories obtained for $St=0.78$. Through visual inspection of the trajectories, one can identify the left and right branches of two coexisting solutions: the basic solution with a spatial period of one, and a new periodic solution with spatial period of three. We call this new solution a *subharmonic*-3 one, and generally solutions with spatial period *n subharmonic-n*.

The subharmonic-3 solution is stable only over the limited range $0.78<St<0.926$. By further increasing St to 0.93, the subharmonic-3 solution can no longer be observed, and only the basic solution is stable, as shown in Fig. 2(h).

A third bifurcation is observed for St between 0.93 and 0.95. In this case, the newly generated secondary solution is a subharmonic-2 solution shown with both left and right branches in Fig. 2(i), along with the basic solution.

For $St>1$, the complexity of the particle dynamics grows rapidly as it becomes increasingly dominated by inertial forces. As will be demonstrated below in detail, two main processes can be identified: firstly, additional subharmonic-2 solutions are created by successive bifurcations. These new solutions coexist with each other and the basic solution, thereby enriching the collection of stable trajectories. Secondly, each of these subharmonic-2 solutions undergoes a succession of period doublings *ad infinitum*, thereby transitioning to chaos. Order in the form of a single subharmonic trajectory is reestablished beyond a further critical value of St, before another transition to chaos occurs.

The process of successive bifurcations is shown in Fig. 3 for the flow parameters $k=0.9$ and $\sigma=4.0$. Simulations using 10 to 50 particles initially seeded with the fluid velocity at $y=0$ and $0.01<z<0.17$ (in the downwelling region) al-

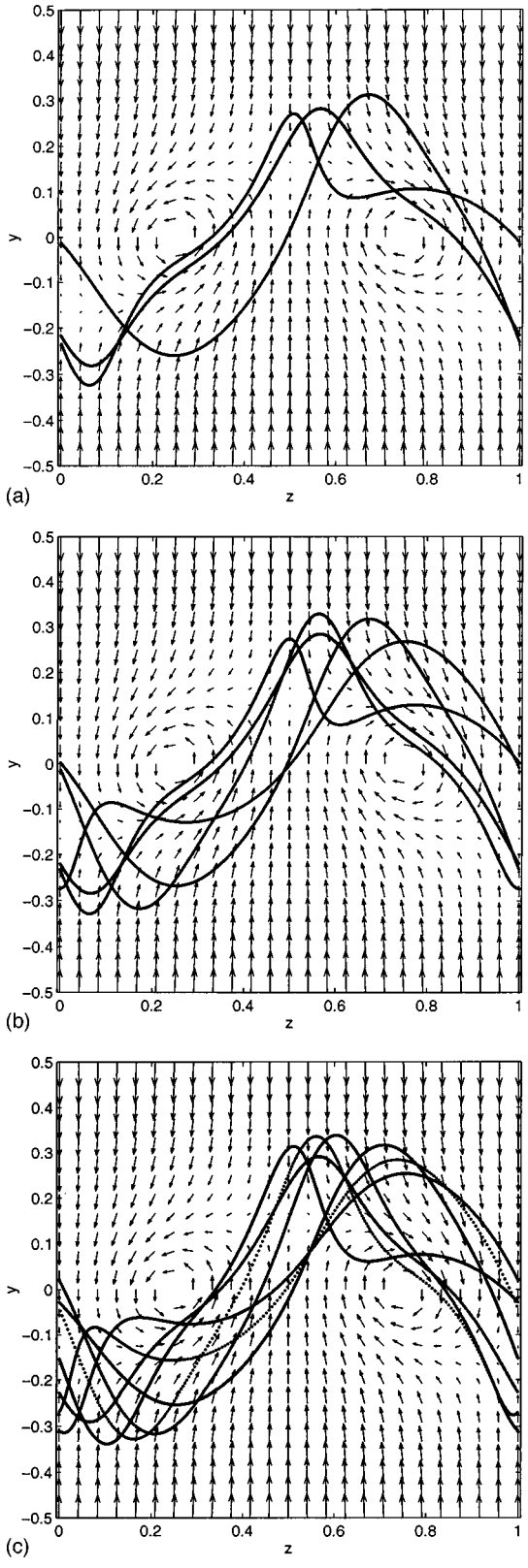

FIG. 3. Successive bifurcations of particle trajectories. $k=0.9$; $\sigma=4.0$. (a) Right branches of particle trajectory solutions for $St=0.95$. A subharmonic-2 trajectory exists along with the basic solution. (b) Right branches of particle trajectory solutions for $St=1.00$. A bifurcation has generated an additional subharmonic-2 trajectory. As a result, three possible stable trajectories exist: one basic and two subharmonic-2 solutions. (c) Right branches of particle trajectory solutions for $St=1.05$. A new bifurcation has led to a third subharmonic-2 solution.

low us to capture the right branches of the multiple existing solutions of Fig. 2(i).

Figure 3(a) shows the right branches of the basic solution and a subharmonic-2 solution for $St=0.95$, a situation similar to that shown in Fig. 2(i). In contrast to previous bifurcations, where subharmonic-3 secondary solutions were created which then dissapeared at higher St values, the additional subharmonic-2 solution remains stable until a new bifurcation occurs. For $St=1.00$, we observe the creation of a new subharmonic-2 solution, allowing for three simultaneous solutions for the particle trajectories to exist: one basic solution and two subharmonic-2 solutions, as shown in Fig. 3(b). A third bifurcation occurs at $St=1.053$, allowing for the existence of four simultaneous solutions: one basic solution and three subharmonic-2 solutions, as shown in Fig. 3(c).

Beyond $St=1.10$, it becomes increasingly difficult to visually distinguish between possible newly emerging subharmonic solutions and previously existing solutions that may have undergone a period doubling bifurcation. In order to understand the mechanisms at work, we hence follow only one of the possible solutions for the particle trajectories. This is achieved by one-particle simulations, starting with the same initial position and velocity for each calculation, varying only the value of St. The initial location is (0.01,0), with the initial particle velocity again being equal to the local fluid velocity. Nevertheless, additional tools are necessary in order to analyze the nature of the computed solutions. By considering the particle motion as a four-dimensional dynamical system in the z, y, $w=\dot{z}$, and $v=\dot{y}$ coordinates, it is possible to project the solutions into the two-dimensional $v=\dot{y},y-$phase plane, and to construct Poincaré sections by recording the $y-$ and $v-$coordinates in the phase plane every time the particle travels one spatial period $\Delta z=1$.

The evolution of a single subharmonic-2 solution with increasing St is shown in Fig. 4. A subharmonic-2 solution, previously generated in the sequence of the successive bifurcations described above, is shown in Fig. 4(a) for $St=1.10$. The corresponding Poincaré section accordingly shows two points. As St is slightly increased to 1.15, this subharmonic-2 solution becomes a subharmonic-4 solution, Fig. 4(b). The corresponding Poincaré section shows four points. Subsequently, a further period doubling occurs, which leads to the presence, at $St=1.167$, of a subharmonic-8 solution (with eight points in the Poincaré section), as shown in Fig. 4(c). This behavior is typical for certain nonlinear dynamical systems,[19] and it rapidly leads to a chaotic solution. Figures 4(d)–4(f) show the evolution of the solution structure until it finally becomes chaotic for $St=1.23$. The corresponding Poincaré section in Fig. 4(f) shows a characteristic chaotic structure. For the slightly increased values of $St=1.25$, order is reestablished in the form of a subharmonic-2 solution [Fig. 5(a)].

The final stages in the evolution of the subharmonic-2 solution are shown in Fig. 5. The subharmonic-2 form of the solution that exists for $St=1.25$ is stable only over a small range of St. It is shown in Fig. 5(a) over eight units in the z-direction, with the cores of the clockwise rotating vortices indicated by filled circles, and those of the counterclockwise rotating ones denoted by empty circles. As St is slightly

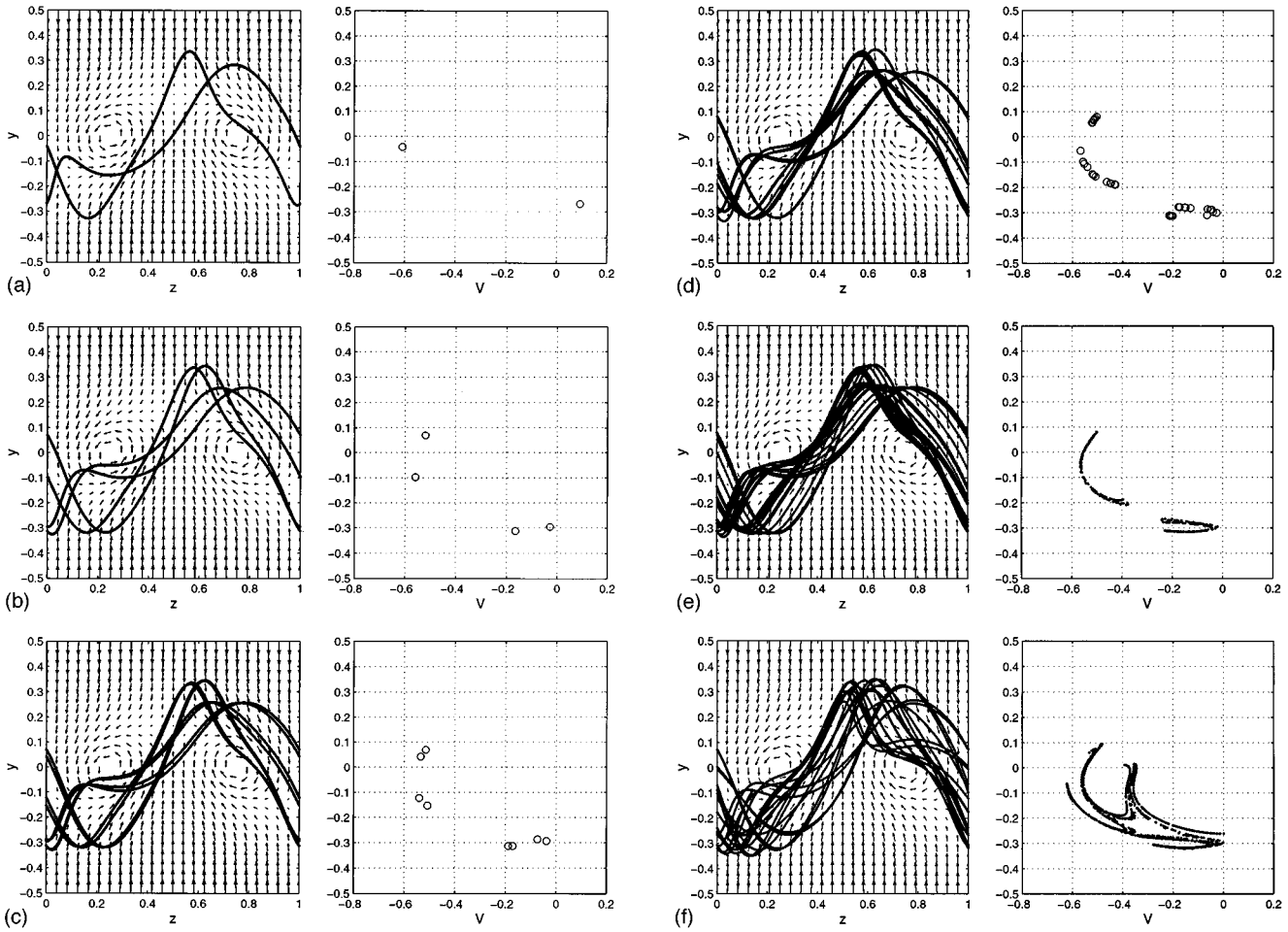

FIG. 4. Successive period doubling for a particle trajectory. $k=0.9$; $\sigma=4.0$. (a) Particle trajectory (left plot) and the corresponding Poincaré section (right plot) for $St=1.10$. The subharmonic solution with a spatial period of two. (b) Particle trajectory and the corresponding Poincaré section for $St=1.15$. First period doubling: subharmonic solution with a spatial period of four. (c) Particle trajectory and the corresponding Poincaré section for $St=1.167$. Second period doubling: subharmonic solution with a spatial period of eight. (d) Particle trajectory and the corresponding Poincaré section for $St=1.184$. Quasi-periodic solution. (e) One particle trajectory and the corresponding Poincaré section for $St=1.19$. Banded chaotic solution. (f) One particle trajectory and the corresponding Poincaré section for $St=1.23$. Chaotic solution.

increased to $St=1.286$, a closed periodic solution is observed, as shown in Fig. 5(b). The physical mechanism which generates this particular form of the trajectory is a certain resonance between the phase shift generated by the inertia of the particle and the forcing flow: The inertia of the particle generates a delay in the particle's response as it follows the flow. It cannot follow the flow as a fluid particle would, as its inertia is continuously altering its trajectory from that of a fluid particle. The particular resonance for the present value of St leads to a situation where the heavy particle follows a trajectory similar to the previous subharmonic one, but only for about a distance of four units. It then switches directions, upon which it travels in the opposite spanwise direction for about four units, before switching again. This solution is stable only over a very narrow range of St. By increasing St to 1.289, the closed solution becomes unstable, and the particle trajectory exhibits intermittency.[20] Here, the particle is captured in a nearly closed trajectory for only a few cycles. It then escapes, travels for a few units in the spanwise direction, and is captured in a different nearly closed loop of similar form. The plot in Fig. 5(c) shows this process.

As St is further increased, the pattern of the closed loop which captures the particle at random from time to time becomes less visible. The particle motion becomes fully chaotic. In Fig. 6(a), such a chaotic particle trajectory is plotted over a distance $\Delta z=8$ for $St=1.32$. In this one-particle trajectory plot, the particle is moving chaotically in both spanwise directions, as it is being turned back and forth at random. The Poincaré section and the particle distribution pattern corresponding to this trajectory are shown in Fig. 6(b). While the chaotic structure in the two-dimensional phase space is similar to that found for $St=1.23$ [Fig. 4(f)], with additional spiral forms, the distribution of the particles no longer shows a strong particle concentration along preferred paths and the regions near the vortex centers are depleted of particles. A simulation using 32 pairs of particles was performed in order to compute the Lyapunov exponent of the trajectories. The particles were initially placed at random locations in the flow with a distance of 10^{-6} between

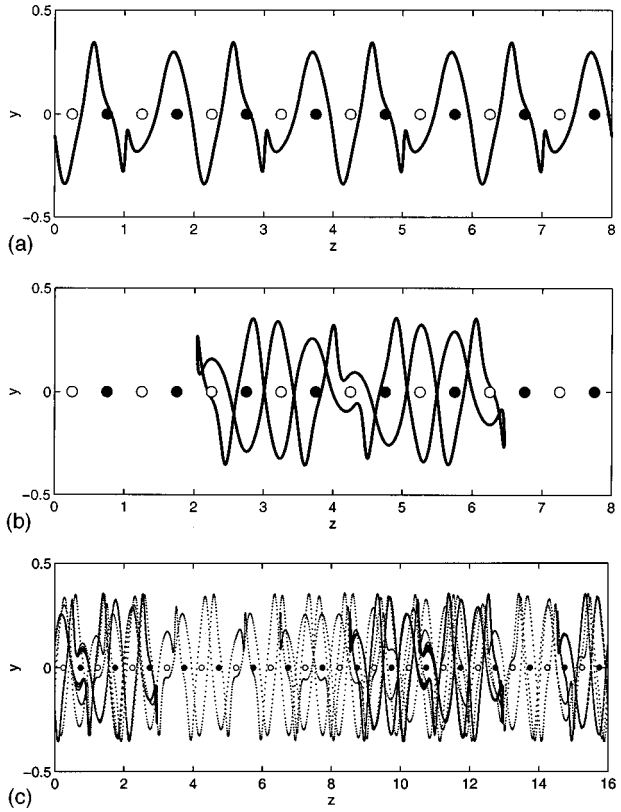

FIG. 5. Onset of chaotic behavior for a particle. (a) Subharmonic-2 solution for $St=1.25$. The empty and filled circles mark the left and right rotating vortices. (b) Particle trajectory for $St=1.286$. A closed loop solution results from periodic switching of directions. (c) Particle trajectory, $St=1.289$. *Intermittency*: the particle remains attracted by the closed loop trajectory only for a limited number of periods, then escapes, eventually being recaptured later by another closed loop, where it is trapped again for a limited number of periods.

the particles of each pair. All pairs were tracked in time, simultaneously, and the distance between the particles of each pair renormalized periodically. The growth of the distance with time is shown in Fig. 6(c), averaged for all 32 particle pairs. The diagram indicates a Lyapunov exponent of 0.06662. The variation of the Lyapunov exponent with St is shown in Fig. 6(d). A maximum is observed around $St=3$.

It is important to notice that it is not the process of period doubling ad infinitum that leads to the final onset of chaotic motion, but rather the inability of the particle to establish a consistent direction of motion, which leads to random directional switches.

B. Particle behavior at low strain

Our scaling analysis[1] for σ shows that when the counterrotating streamwise vortices are fully developed and reach a strength comparable to that of the spanwise Kelvin-Helmholtz vortices, the value of the dimensionless strain rate reaches a minimum of $\simeq 2$. The term of ''low strain'' therefore indicates a reduced strength of the strain component of the fluid motion as compared to the vortex related component. Such low strain can only trap very small particles at the vortex centers. For $\sigma=2$, the critical value for the Stokes number[1] is $St_{cr}=0.0011$. Particles with $St=0.005$ collect along small, nearly circular trajectories around the vortex centers, as shown in Fig. 7(a), similar again to the case of an axisymmetric Burgers vortex,[17] in spite of the present plane strain. Lin and Corcos[6] suggest that the fully developed streamwise vortices ''feel'' a radially averaged strain, which corresponds to Neu's[21] solution for the asymptotic state of a vortex under plane strain, which shows a similarity with the Burgers vortex model. Keeping this in mind, it is to be expected that the particle dynamics in the vicinity of the streamwise vortices in plane strain resembles that found around a Burgers vortex.[18]

As St increases, the closed loops formed by the particles around each vortex become larger [Fig. 7(b)], until they break up and form open periodic trajectories, corresponding to the above basic solution, with left and right branches [Fig. 7(c)]. No further bifurcations are observed at this low σ, as St is increased and the open trajectories acquire larger amplitudes. As shown in Fig. 7(d), for St values as high as 4.0 the trajectory is still stable.

The transition to the chaotic regime of motion occurs gradually, as fewer and fewer particles asymptotically approach periodic trajectories. As shown in Fig. 7(e), while most of the particles still collect along the periodic trajectory, a significant number of them continue to move chaotically, even for long times. The pattern shown in Fig. 7(e) remains the same, even if the simulation is carried out to fivefold larger times. We hence conclude that under the present conditions transition to chaos is the result of a gradual shrinking of the basin of attraction of the single existing periodic solution.

As St is further increased, the contour of the basic solution trajectory gradually ''dissolves'' in the particle distribution snapshots. Eventually, all particles move chaotically, as shown in Fig. 7(f) for $St=4.75$.

C. Particle behavior at high strain

High values of the strain parameter correspond to the early stages of development of the streamwise vortices, when their strength is a small fraction of that of the spanwise vortices. To study this regime, we employ a value of $\sigma=13$.

At this intense strain, the critical[1] St value is 0.0077. For $St=0.005$, the accumulation process is shown in the succession of particle position snapshots in Fig. 8. Initially, all particles rapidly collect in a narrow band, as shown in Fig. 8(a). This band is located slightly above and below the level of the vortex row. It grows continuously narrower at a slower rate [Figs. 8(b) and 8(c)] and becomes entrained into the vortex centers. Subsequently, it is slowly being depleted [Fig. 8(d)], as particles are transported towards the vortex cores. The initial band formation proceeds on a fast time scale, as it is caused by the strong strain induced fluid velocity. The strain keeps the particles within the narrowing band, which passes through the flow stagnation points. The actual particle accumulation at the vortex centers is then accomplished by the vortex induced velocity. Since the vortices are relatively weak, this second part of the process is slow. In a real, three-dimensionally evolving flow, one would expected that during this time the vortices will strengthen, so that the rotational velocities that they induce will become stronger.

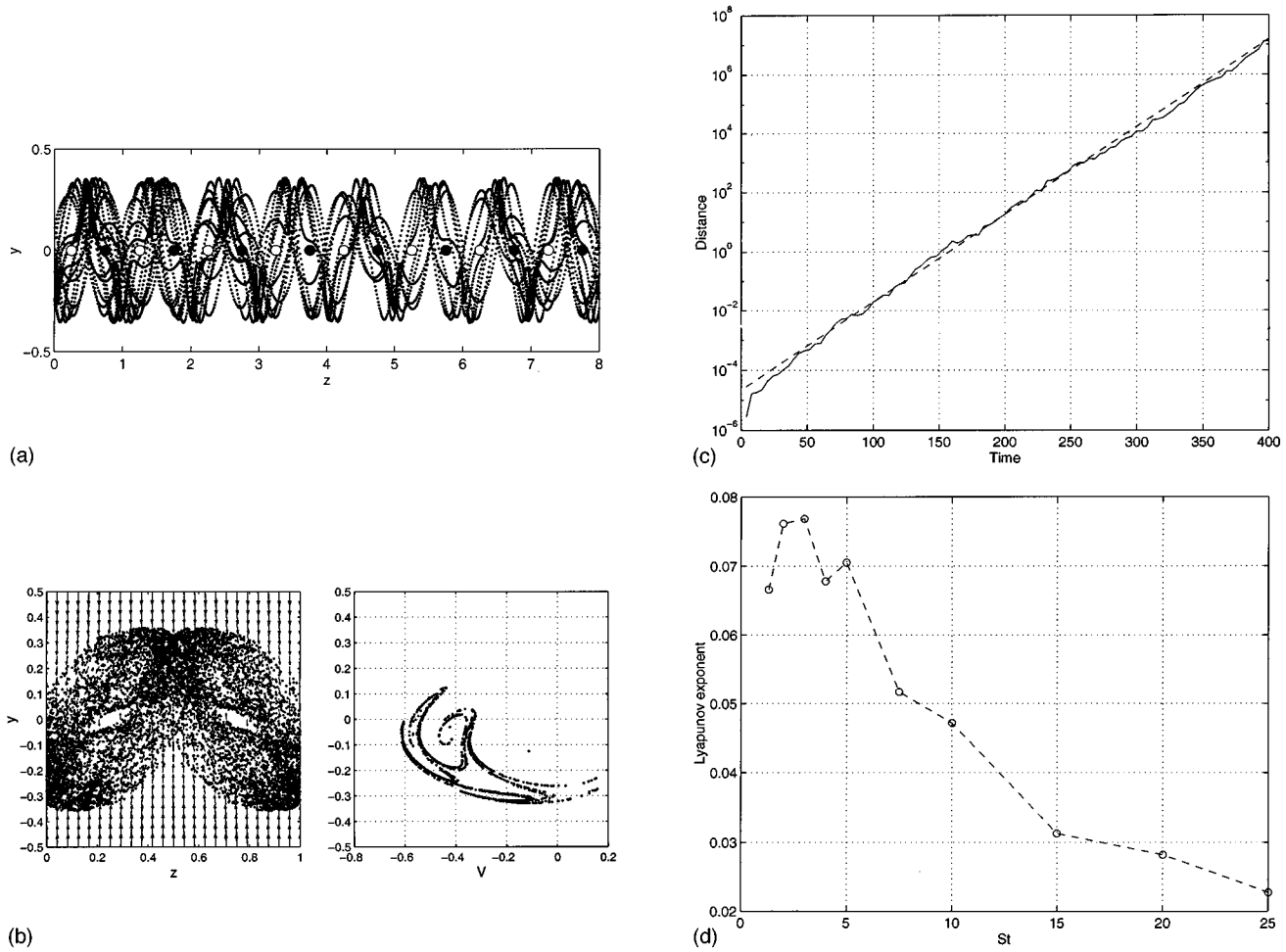

FIG. 6. The particle dynamics in the chaotic regime. Here $k=0.9$; $\sigma=4.0$. (a) Chaotic particle trajectory $St=1.32$. (b) Particle distribution for $St=1.32$ (left plot) and the corresponding Poincaré section in the (y,v)-phase space (right plot). (c) Lyapunov diagram for $St=1.32$. (d) Variation of the Lyapunov exponent with the particle St values. A maximum can be observed at $St=3.0$.

For St values larger that the accumulation limit, closed trajectories are formed around each vortex. At high strain rates, the first bifurcations leading to secondary solutions for the particle trajectories occur before the closed loops are broken open, so that the newly generated trajectories are closed as well. In Fig. 9(a), two stable closed loops are shown around each vortex.

As St increases, each of the two loops starts a period doubling process. In Fig. 9(b), for $St=0.25$, one of the closed trajectories is still a simple loop, while the other has split in two interconnected loops. For $St=0.30$ both loops previously observed in Fig. 9(a) have split into two interconnected loops each [Fig. 9(c)]. The period doubling continues until the chaotic regime is reached, as shown in Fig. 9(d).

The opening of the closed chaotic trajectories occurs around $St=0.5$, as shown in Fig. 9(e). For $St=0.75$, the chaotically moving particles still form relatively narrow bands, due to the strong strain. These bands, shown in Fig. 9(f), allow intense spanwise particle transport.

IV. GRAVITY EFFECTS

Under certain circumstances, gravity is expected to lead to particle accumulation.[1] In the following, we will demonstrate the effects of gravity on the trajectories described in Section III for the moderate strain parameter value $\sigma=4.0$. The concentration of vorticity is again characterized by $k=0.9$.

The general observation is that gravity deforms the previously observed trajectories. Figure 10 shows the evolution of the trajectory's shape under increased gravity for $St=0.20$. At $Fr=10.0$, the effect of the gravity is barely felt, and the particle trajectory has a shape that is very similar to that in the absence of gravity [cf. Fig. 2(a)]. Also shown are the equilibrium points for the particle, which for the present parameters are unstable and located very close to the vortex centers and the stagnation points.

For $Fr<1.0$, the effects of gravity become apparent, as small secondary loops form near the upper corner of the trajectory [Fig. 10(b)]. The symmetry with respect to the center of the vortex is rapidly destroyed by gravity, and the displacement of equilibrium points from the vortex centers and flow stagnation points is observable.

The deformation of the initial trajectory continues for decreased Fr values, until it touches the neighboring trajectory. Even lower values of Fr lead to trajectories that form a double loop around a pair of counterrotating vortices [Fig.

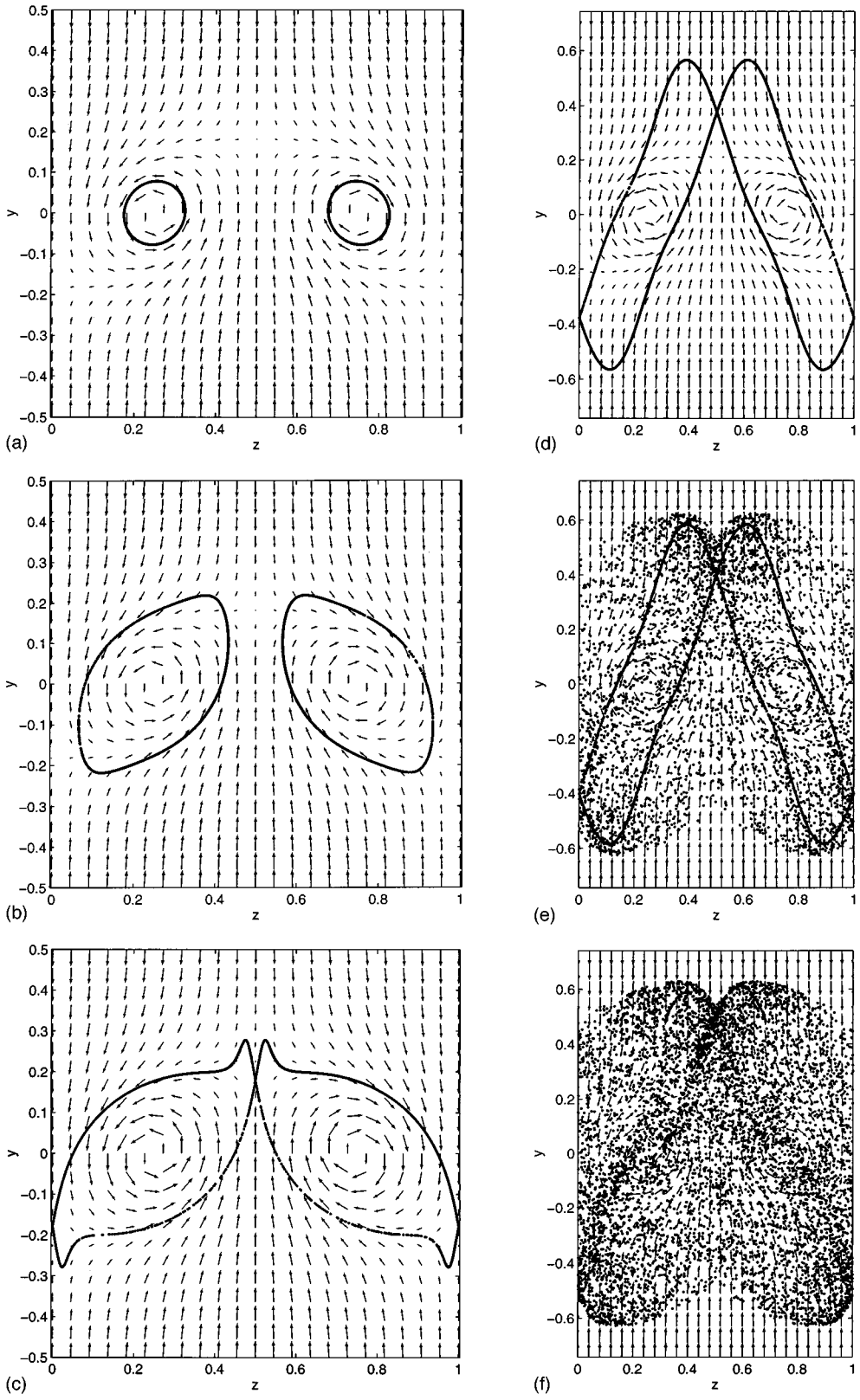

FIG. 7. I. Particle trajectories at low strain. (a) $\sigma=2.0$; $k=0.9$; $St=0.005$. Particles collect along closed, nearly circular orbits. (b) $\sigma=2.0$; $k=0.9$; $St=0.1$. Increased inertia enlarges the collection orbits. While similar in size to those shown in Fig. 2(a) for $\sigma=4.0$, the present orbits form at half the St value, and they are rounder in shape. (c) $\sigma=2.0$; $k=0.9$; $St=0.25$. Particles collect along an open periodic trajectory corresponding to the basic solution. (d) $\sigma=2.0$; $k=0.9$; $St=4.0$. All particles collect along one open unique trajectory corresponding to the basic solution. II. Particle dispersion: the onset of chaotic behavior at increased particle inertia. (e) $\sigma=2.0$; $k=0.9$; $St=4.6$. While a number of particles still collect along the open, unique trajectory, other particles do not asymptotically approach any periodic trajectory. (f) $\sigma=2.0$; $k=0.9$; $St=4.75$. No coherent solution exists for the trajectories, all particles move chaotically.

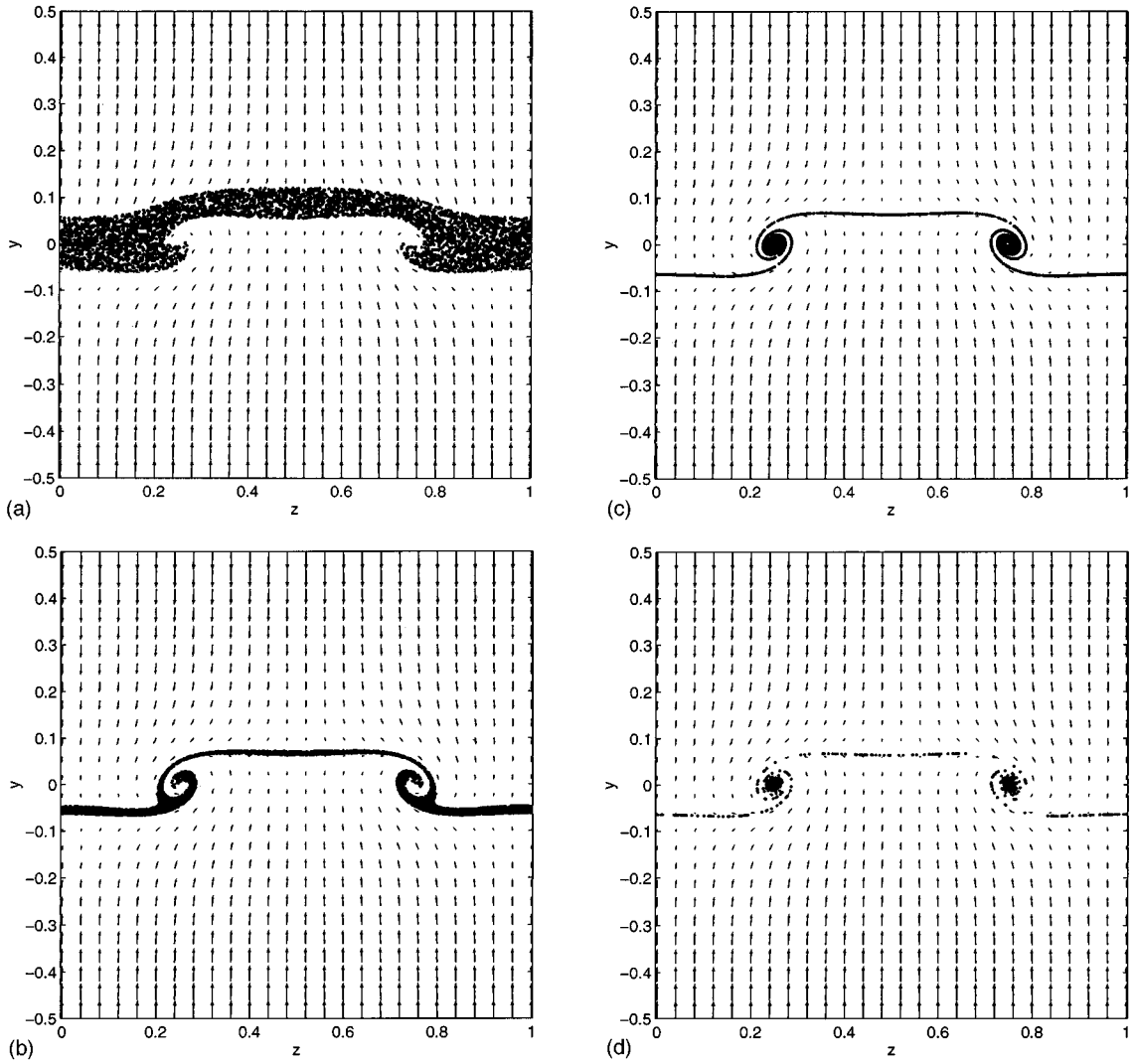

FIG. 8. Accumulation of particles at the center of the counterrotating vortices, under conditions of high strain $\sigma=13.0$. Here $St=0.005$. (a) $t=0.1275$. All particles are rapidly collected within a narrow band along the row of vortices. (b) $t=0.252$. The band of particles is narrowing continuously under the influence of strain in the flow field. (c) $t=0.752$. The band of particles has been narrowed to a thin line. The particles are gradually entrained into the vortex centers. (d) $t=1.752$. The band is gradually depleted of particles which accumulate at the center of vortices.

10(c)]. The break-up due to increased gravity is fundamentally different from the break-up due to increased inertia observed earlier. There the symmetry of the trajectory with respect to the vortex center was fully preserved through the bifurcation, which led to a periodic open trajectory. Increased gravity, on the other hand, results in trajectories that are still closed, and no longer symmetric with respect to the vortex centers. However, the symmetry with respect to the vertical axis is maintained. By further increasing gravity, we reach a threshold beyond which the condition[1] $St/Fr^2>k$ is satisfied, so that the particles accumulate at the now stable equilibrium point on the $z=0.5$ axis just below the row of vortices [Fig. 10(d)]. Based on our earlier stability results,[1] this behavior is to be expected, as no other stable equilibrium points exist for the present parameters.

The deformation of an open, periodic trajectory under gravity is depicted in Fig. 11 for $St=0.30$. For $Fr=10$ [Fig. 11(a)], the trajectory is hardly affected by gravity [cf. Fig. 2(c)]. At $Fr=1$, it has undergone a bifurcation to a closed double loop trajectory [Fig. 11(b)], which for even lower Fr is further deformed [Fig. 11(c)], until the accumulation condition $St/Fr^2>k$ is satisfied and the particle comes to rest at the stable equilibrium point [Fig. 11(d)].

For particles characterized by larger St values, the phenomena associated with increased gravity levels become more complex. As an example, we present the modification of an initially subharmonic-3 particle trajectory by gravity. Figure 12(a) shows the trajectory, along with the associated Poincaré section, for low levels of gravity ($Fr=10$) and $St=0.78$. The Poincaré section shows three distinct points, confirming the subharmonic-3 nature. As gravity is increased, the trajectory is deformed, and its periodicity is altered. In Fig. 12(b), for $Fr=1.72$ the trajectory is quasi-chaotic. The Poincaré section shows a large number of points, but the trajectory is limited to a small fraction of the computational domain. For further increased gravity, corresponding to $Fr=1.68$, the trajectory becomes periodic again, displaying a spatial period of 2, as shown in Fig. 12(c). We

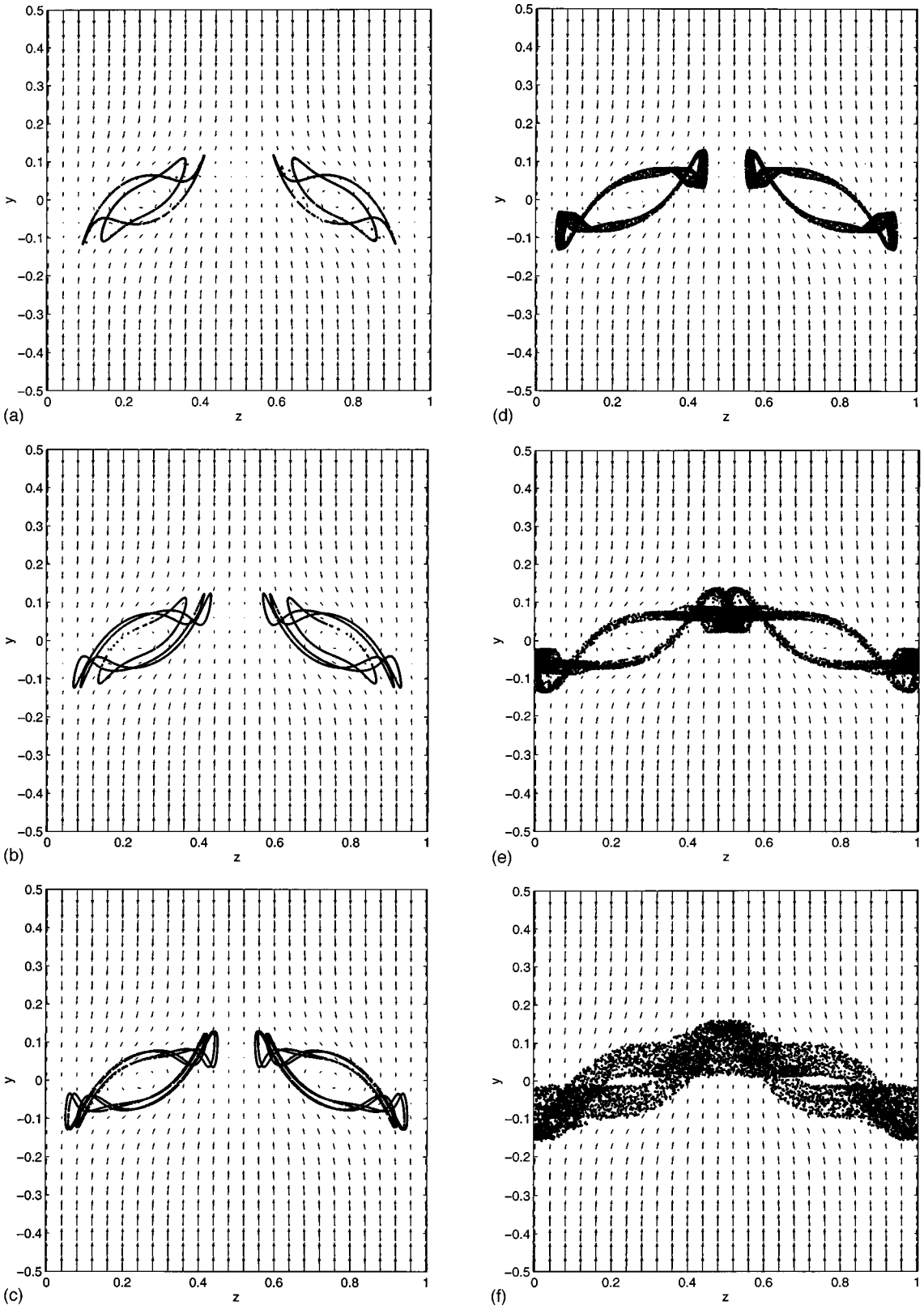

FIG. 9. Particle dispersion at high strain. (a) $\sigma=13.0$; $k=0.9$; $St=0.2$; All particles collect along two closed, periodic trajectories around each vortex. (b) $\sigma=13.0$; $k=0.9$; $St=0.25$. A bifurcation leads to a period doubling of one of the closed loops. (c) $\sigma=13.0$; $k=0.9$; $St=0.30$. For these parameters, both of the closed loops are of subharmonic nature. (d) $\sigma=13.0$; $k=0.9$; $St=0.35$. Mutliple bifurcations allow for the production of a band of trajectories until the chaotic regime is reached. However, particle dispersion is limited to a narrow closed chaotic region. (e) $\sigma=13.0$; $k=0.9$; $St=0.5$. For increased inertia, the closed, chaotic trajectory beaks up into an open chaotic trajectory, with left and right branches. (f) $\sigma=13.0$; $k=0.9$; $St=0.75$. The chaotic trajectory is widening with increased particle inertia, forming bands of particles whcih allow intense spanwise transport of material.

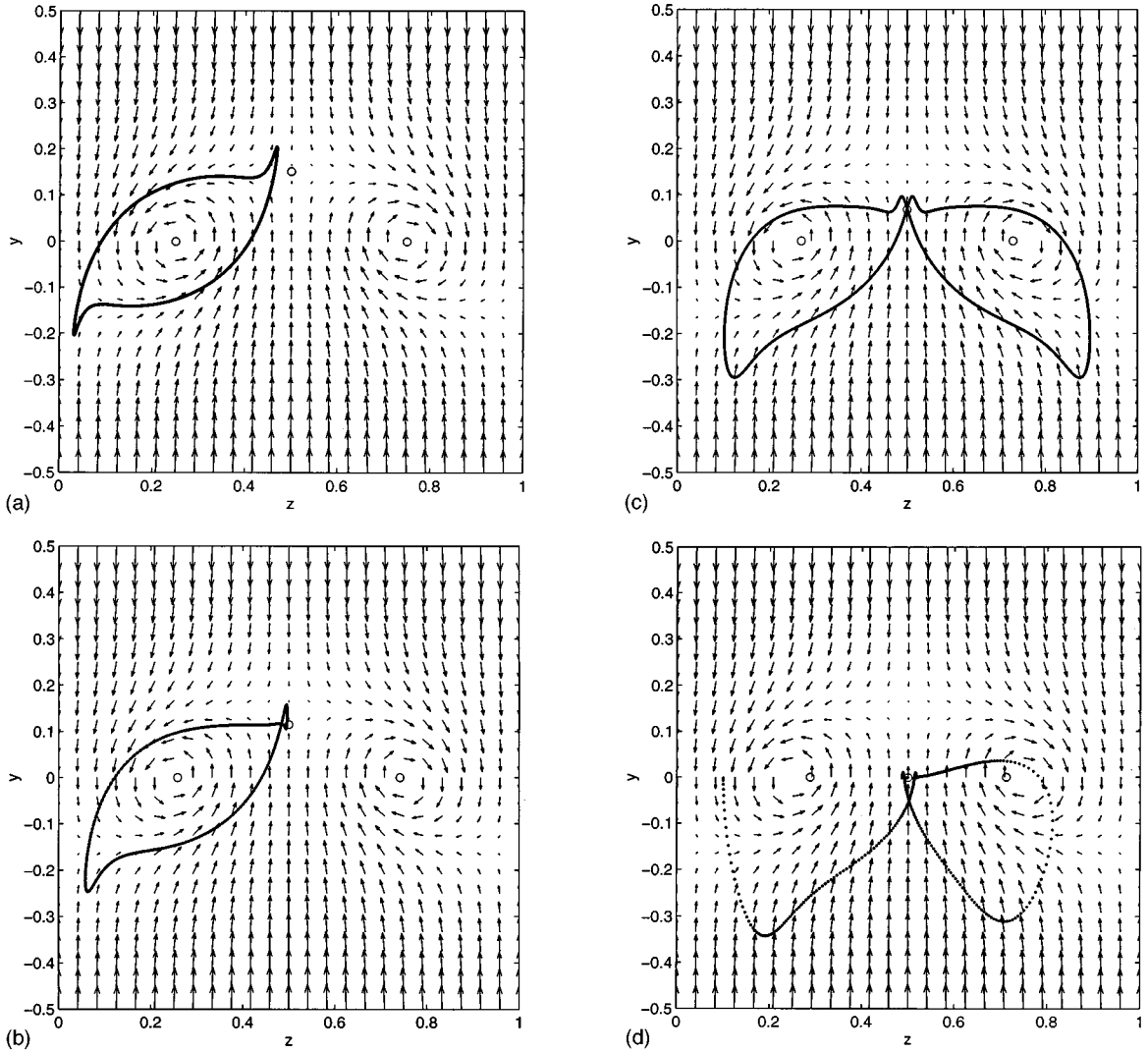

FIG. 10. The effect of gravity on a particle trajectory at moderate strain. Flow parameters: $k=0.9;\sigma=4.0$. The circles indicate the location of the equilibrium points. (a) $St=0.20;Fr=10.0$. Closed loop trajectory around one counterclockwise rotating vortex. (b) $St=0.20;Fr=0.90$. Increased gravity deforms the shape of the closed trajectory and breaks its symmetry. (c) $St=0.20;Fr=0.60$. Closed trajectory around both counterrotating vortices. (d) $St=0.20;Fr=0.47$. The particle is driven towards the equilibrium position.

thus find that, under increasing gravity, the initial subharmonic-3 trajectory is transformed into a subharmonic-2 trajectory, after passing through quasi-periodic intermediate state.

The alteration of the trajectory form continues with the closing of the trajectory, at a gravity level corresponding to $Fr=1.15$. In Fig. 12(d), the periodic closed trajectory is shown in a plot extending over eight counterrotating vortex pairs. The closed loop extends over four counterrotating vortices, while maintaining symmetry with respect to the vertical line midway between the vortices of the inner pair. Slightly increased gravity levels ($Fr=1.10$) render the closed loop unstable and generate a random motion of the particle. By further increasing gravity, we eventually again reach a threshold beyond which the accumulation criterion $St/Fr^2>k$ is satisfied, so that the particle comes to rest at a stable equilibrium point [Fig. 12(f)].

V. STATISTICAL MEASURES FOR THE DISPERSION OF HEAVY PARTICLES

A. Dispersion in the absence of gravity

In the following, we will present statistical information regarding the particle concentration fields generated by counterrotating strained vortices. In order to obtain this information, we carried out simulations with 1,000 particles for various St values in the range of $1.5<St<25$. The particles were initially randomly seeded in the upper half of the computational domain and then tracked for 5000 time steps. To avoid any effects due to the initial conditions, the particle positions were recorded only for the last 1,000 time steps. Since for the present range of St the particle motion is chaotic, the 10^6 positions recorded over time for 10^3 particles have the same distribution as the positions of 10^6 different particles recorded in an instantaneous snap-shot. A two-dimensional

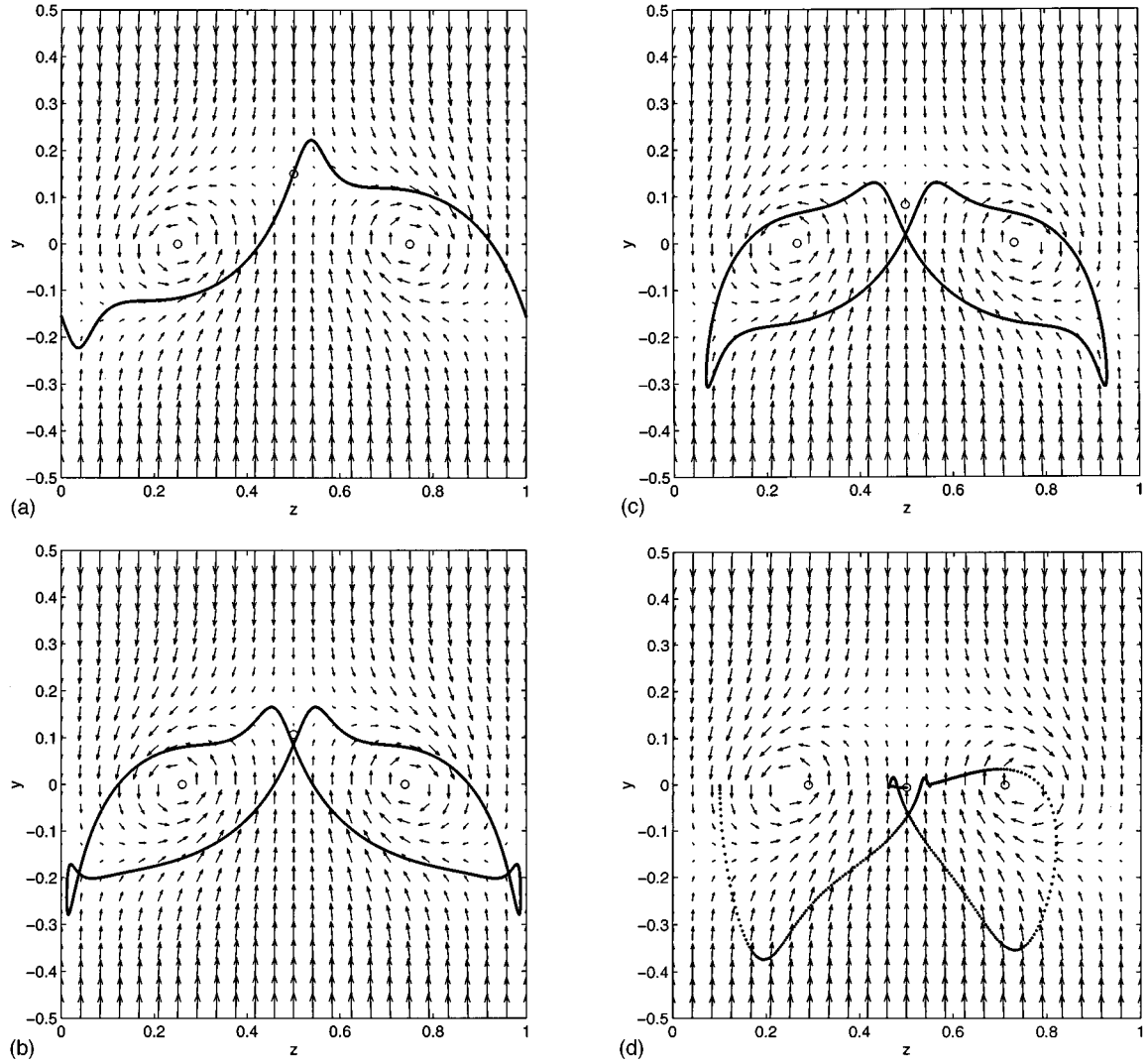

FIG. 11. The effects of gravity on particle trajectory at moderate strain. Flow parameters: $k=0.9;\sigma=4.0$. (a) $St=0.30;Fr=10.0$. Open, periodic trajectory corresponding to the basic solution. (b) $St=0.30;Fr=1.0$. Gravity deforms the shape of the basic trajectory into a closed double loop trajectory around a pair of counterrotating vortices. (c) $St=0.30;Fr=0.80$. Increased gravity further deforms the double loop trajectory. (d) $St=0.30;Fr=0.57$. The particle is driven towards the equilibrium position.

probability distribution function $C_{pdf}(z,y)$, equivalent to the particle concentration field, can be computed from the 10^6 recorded locations by dividing the computational domain into square bins of size $\Delta=0.01$ and counting the number of particles in each bin. A typical pdf is shown in Fig. 13 for $St=25$. Darker gray shades indicate higher particle concentrations, or, equivalently, a higher probability to find a particle in a certain bin. In order to obtain information on the cross-stream particle distribution $D(y)$, we integrate in the z-direction and normalize in such a way that the concentration would be unity if the particles were distributed equally between $y=-1$ and $y=1$. This normalized distribution D is shown in the right half of Fig. 13.

The ability of the counterrotating vortices to eject particles can be quantified by the width δ of the cross-stream distribution, which represents the distance between the extreme locations at which particles can still be found, as indicated in Fig. 13. A further important qualitative aspect of the dispersion is its non-uniformity γ, which is expressed as the ratio of the maximum D_{max} of the cross-stream distribution and its average value D_{avg} between the extreme locations

$$\gamma=\frac{D_{max}}{D_{average}}. \tag{10}$$

The variation of the cross-stream distribution width δ as a function of St is shown in Fig. 14(a) for the flow parameters $k=0.9$ and $\sigma=4.0$. By comparing the data with the dotted line, whose slope is 1/4, we find the approximate scaling law,

$$\delta\sim St^{1/4}. \tag{11}$$

Similarly, Fig. 14(b) shows the variation of the cross-stream distribution width δ as a function of the strain parameter σ, for $St=10$ and $k=0.9$. By again comparing with straight lines of given slopes, we find a relationship,

$$\delta\sim\sigma^{p}, \tag{12}$$

where the slope p is in the range $-1/3<p<-1/4$.

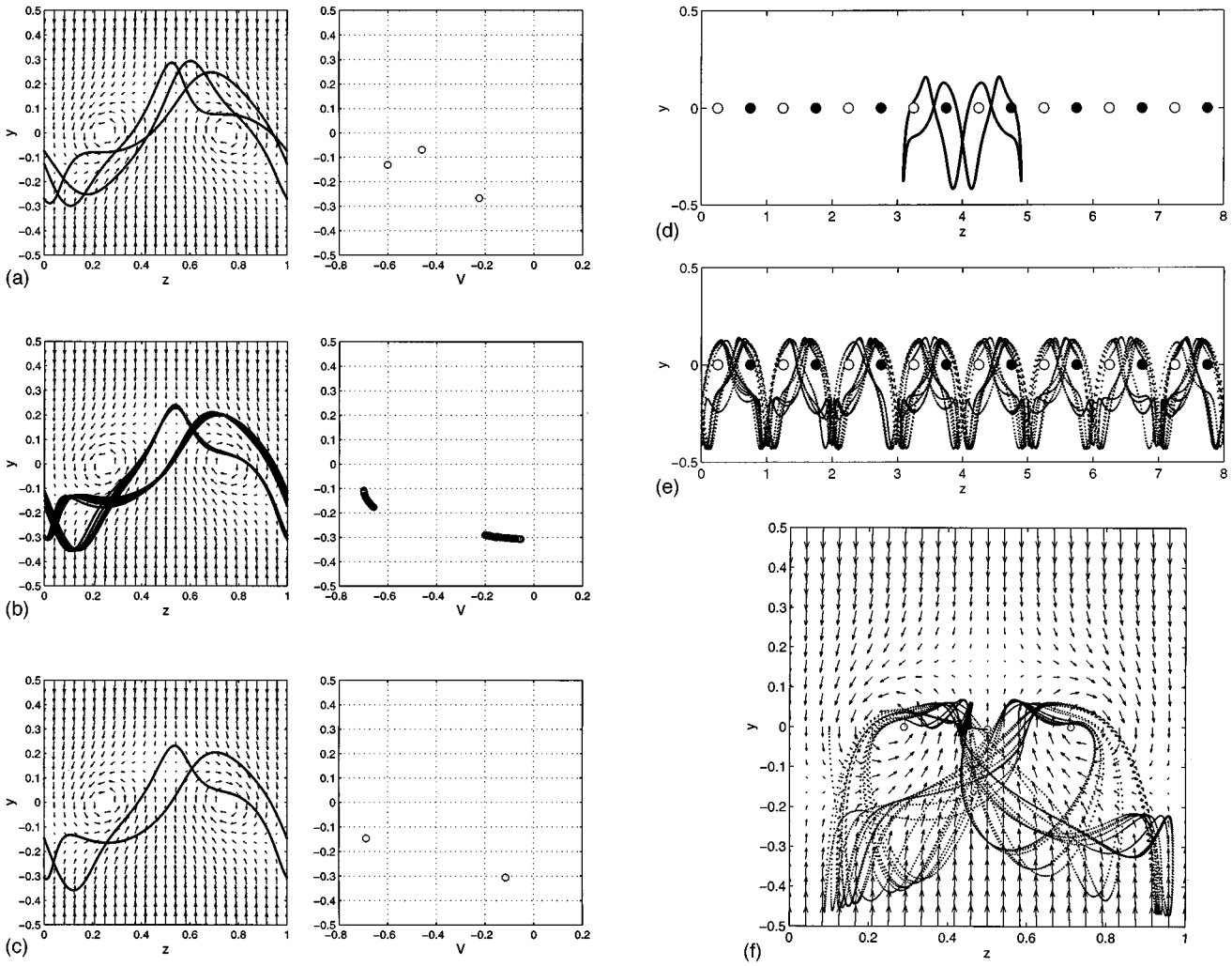

FIG. 12. The effects of gravity on a particle trajectory. I. Change of period of a subharmonic solution. $k=0.9;\sigma=4.0$. (a) Particle trajectory and the corresponding Poincaré section for $St=0.78;Fr=10.0$. Subharmonic solution with a spatial period of 3. (b) Particle trajectory and the corresponding Poincaré section for $St=0.78;Fr=1.72$. Quasi-chaotic solution. (c) Particle trajectory and the corresponding Poincaré section for $St=0.78;Fr=1.68$. Subharmonic solution with a spatial period of 2. II. closing the periodic subharmonic-2 trajectory, onset of chaotic behavior, and accumulation. Here $k=0.9;\sigma=4.0$. (d) Particle trajectory, for $St=0.78;Fr=1.15$. Periodic closed trajectory, with vertical symmetry axis. (e) Particle trajectory, for $St=0.78;Fr=1.10$. Chaotic motion with random direction changes. (f) $St=0.78;Fr=0.92$. The particle comes to rest at the stable equilibrium point.

The above scaling laws can be explained on the basis of a simplified model, for which the particle motion can be found analytically. This model consists of one-dimensional particle motion in a modified fluid velocity field. Specifically, the one-dimensional fluid velocity field contains the strain component plus a forcing component intended to model the effect of the vortices. This forcing component always points in the direction of the particle motion, i.e., it changes direction when the particle changes its direction. In this way, it emulates the upwelling and downwelling regions through which the particle travels alternatingly. The strength of the forcing velocity B is constant and will be specified below. The fluid velocity then has the following form:

$$v_f=\begin{cases}+B-\sigma y_p, & \text{if } v_p>0,\\ -B-\sigma y_p, & \text{if } v_p<0.\end{cases}$$

This approximation gives rise to a linear problem for the particle motion. In order to obtain an expression for the distribution width δ in this model problem, we need to deter-

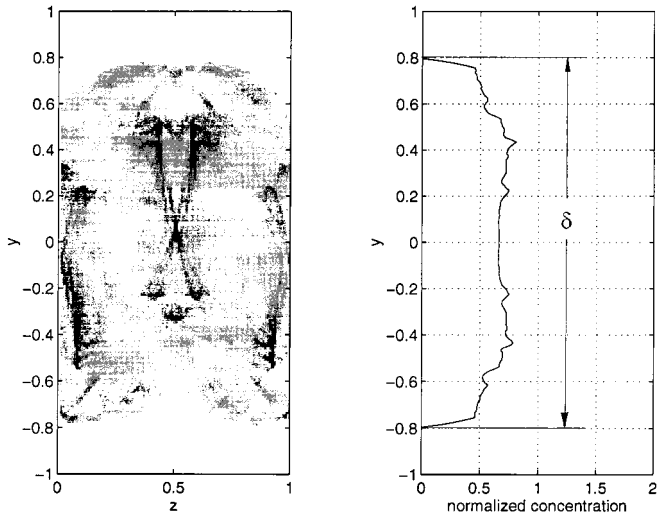

FIG. 13. The probability distribution function for particle concentration (left) with corresponding cross-stream particle distribution (right), for $St=25;k=0.9;\sigma=4.0$.

mine the maximum location y_0 that the particle reaches during periodic motion. By symmetry, the minimum location is $-y_0$, so that the distribution width δ is $2y_0$. To obtain y_0, we assume that the particle starts from y_0 with zero initial velocity. The value of y_0 can then be obtained by requiring that the minimum location of the particle be $-y_0$. The resulting equation of motion for the particle is

$$\ddot{y}_p=\frac{1}{St}(-B-\sigma y_p-\dot{y}_p),$$
$$\dot{y}_p(t=0)=0; \qquad y_p(t=0)=y_0. \tag{13}$$

We are interested in the chaotic motion of fairly heavy particles, so that we can assume $St>1/(4\sigma)$. The solution then takes the form

$$y_p=(y_0-c)e^{-t/2St}\cos(\omega t)+\frac{(y_0-c)}{2St\omega}e^{-t/2St}\sin(\omega t)+c,$$
$$c=-\frac{B}{\sigma} \qquad \omega=\frac{\sqrt{4\sigma/St-1/St^2}}{2}. \tag{14}$$

We now specify the constant model fluid velocity B as the average of the actual vortex-induced velocity between $-y_0$ and y_0. We obtain

$$B=\frac{k}{4y_0},$$

which yields

$$y_{min}=-(y_0-c)e^{-\pi/2St\omega}+c.$$

Since

$$y_{min}=-y_0,$$

we obtain

$$y_0^2=\frac{k}{4\sigma}\left(\frac{1+e^{-\pi/2St\omega}}{1-e^{-\pi/2St\omega}}\right). \tag{15}$$

The exponential terms in the above equation can be expanded for large values of St to obtain

$$\delta=2y_0=\left(\frac{2k}{\pi}\right)^{1/2}(St)^{1/4}(\sigma)^{-1/4}.$$

We thus arrive at a scaling law for the distribution width which is in good agreement with (11) and (12), as far as the dependence on St and σ is concerned. Notice, however, that both our full model for the braid region, as well as the present simplified model, employ a linear strain induced velocity that grows with y without limits. Hence, far away from the vortex row this is not a very accurate representation of the actual three-dimensional mixing layer. Consequently, the above scaling laws (11), (12) can be expected to hold only if δ is not too large, i.e., for St not too large.

Figure 14(c) shows the variation of the non-uniformity measure γ as defined by (10) with St. Its non-monotonic dependence on St indicates that at various intermediate values of St the particle distribution in the braid region becomes quite nonuniform. This is also reflected in the pdf plot of Fig. 13. We notice several dark streaks which indicate larger particle concentrations. These are due to the fact that the random switchbacks occur at preferred locations within the spatial period, and that the particles have small velocities when they undergo a directional reversal, so that they spend a relatively long time near those locations.

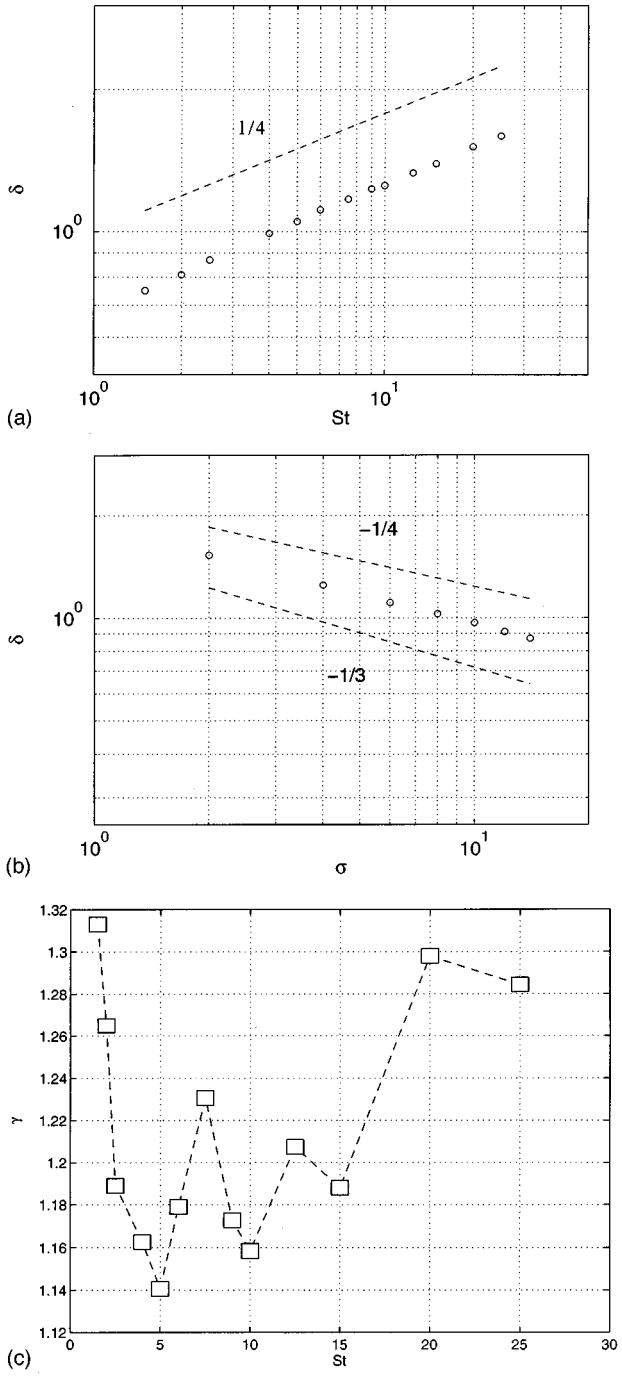

FIG. 14. (a) The variation of the dispersion width δ as a function of St in the absence of gravity for $k=0.9$ and $\sigma=4.0$. For comparison, the dotted line has a slope of 1/4. (b) The variation of the dispersion width δ as a function of σ in the absence of gravity for $k=0.9$ and $St=10.0$. The dotted lines have slopes of $-1/4$ and $-1/3$. (c) The variation of the nonuniformity γ as a function of St in the absence of gravity. Here $k=0.9, \sigma=4.0$.

B. Gravity effects

1. Modification of the particle dispersion field

While we showed earlier that periodic open particle trajectories are altered and eventually broken up and closed by increasing gravity, the chaotic trajectories, with their random switches of direction, can display more complex effects under gravity. It is to be expected that under gravity the entire cross-stream distribution function will be displaced towards negative y-values and undergo an asymmetric deformation.

Typical changes in the dispersion field for particles characterized by high inertia ($St=25$) are presented in Fig. 15. For relatively weak levels of gravity corresponding to $Fr=8$ [Fig. 15(a)], the pdf plot as well as the cross-stream distribution function show a slight downward displacement. In addition, both show a slight asymmetry. However, the dispersion width δ remains nearly unchanged by the present weak level of gravity.

A pronounced effect of gravity can be observed for $Fr=7$ in Fig. 15(b). A large number of particles have collected along statistically preferred trajectories, visible in the form of coherent dark streaks in the two-dimensional C_{pdf} image. While these do not affect the dispersion width, they result in significant non-uniformities in the cross-stream distribution function. As gravity increases further to $Fr=6$, the preferred trajectories disappear again [Fig. 5(c)], while both the pdf and the cross-stream distribution function are shifted to lower y-values. The dispersion width remains unchanged.

The above simulations indicate that for constant St the dispersion width δ does not vary with gravity, while the pdf is displaced downward. This displacement can be quantified by tracking the position of the midpoint y_m between the two y-locations at which the cross-stream distribution reaches zero. Further information about the degree of asymmetry can be obtained by comparing y_m to y_{cg}, which denotes the ''center of mass'' of the cross-stream distribution profile

$$y_{cg}=\frac{\int_{-\infty}^{\infty} D\ y\ dy}{\int_{-\infty}^{\infty} D\ dy}.$$

In the absence of gravity, and hence asymmetry, both quantities are zero. As gravity increases, a growing difference between y_m and y_{cg} indicates a larger degree of asymmetry. This is shown in Fig. 16(a) for $\sigma=4$, $k=0.9$, and the two St values of 5 and 25, respectively. For $St=5$, the difference between y_m and y_{cg} remains small with increasing gravity. For $St=25$, this difference increases with gravity, suggesting a growing asymmetry.

Figure 16(b) shows the variation of the non-uniformity with Fr for the same parameters. While γ is relatively low for $St=5$, more pronounced variations occur for $St=25$, with a maximum of over 40% for $Fr=7$. This situation corresponds to that shown in Fig. 15(b), when preferred trajectories exist.

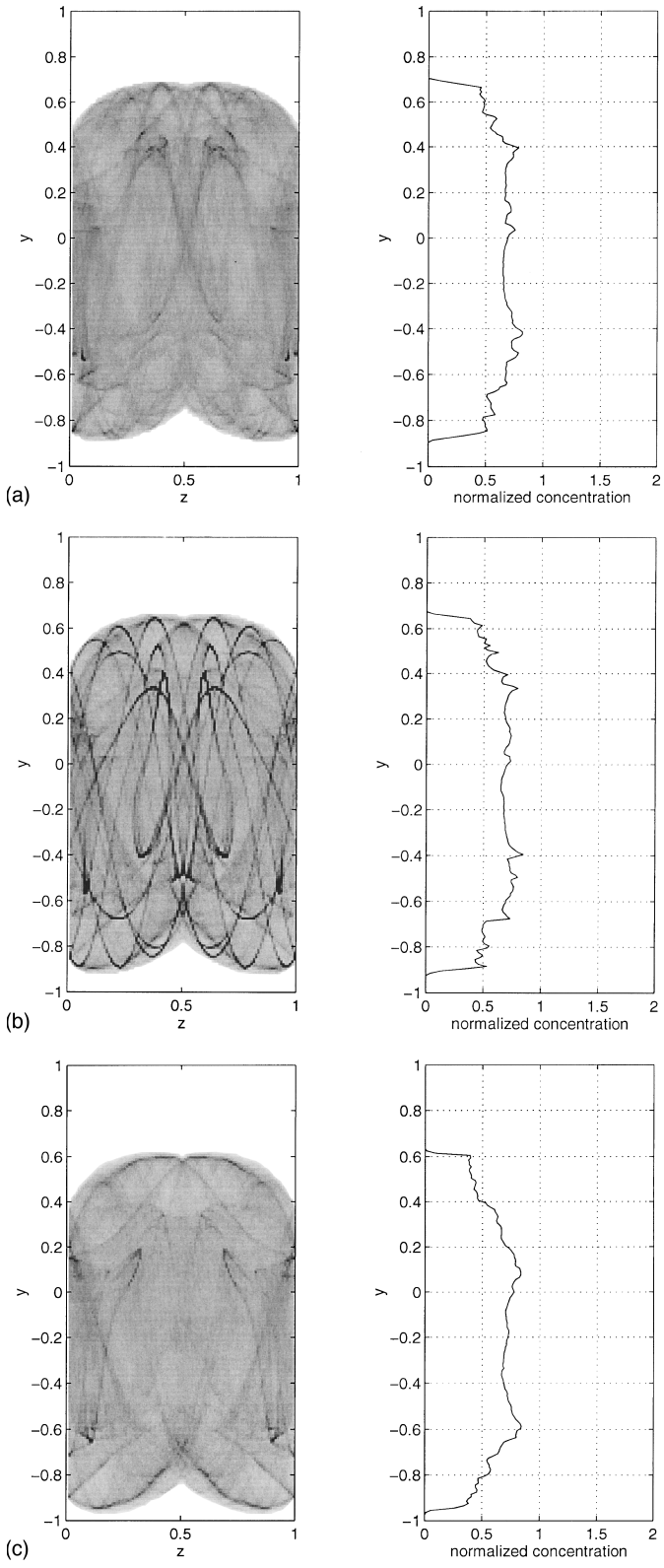

FIG. 15. Probability distribution function and the corresponding cross-stream distribution profile, for flow parameters $k=0.9, \sigma=4.0$ and increased gravity. (a) $St=25, Fr=8.0$; C_{pdf} image (left) and cross-stream distribution profile (right), show no pronounced non-uniformities. (b) $St=25; Fr=7.0$. Dark streaks in the C_{pdf} image indicate coherent particle trajectories, with correspondent sharp peaks in the cross-stream, distribution profile. (c) $St=25, Fr=6.0$. Smooth distribution profile showing visible asymmetry due to stronger gravity.

C. Particle accumulation

As shown in part I of the present investigation,[1] once the accumulation criterion

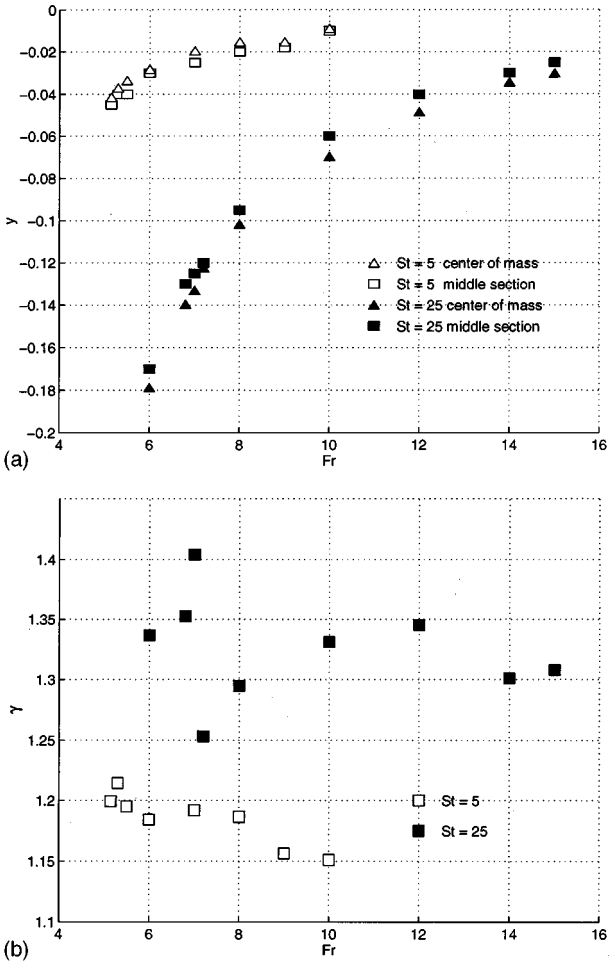

FIG. 16. (a) The variation of the middle-section of the particle dispersion field y_m, and the corresponding "center of mass" of the field y_{cg}, with increased gravity (decreasing Fr values) for $St=5$ and $St=25$. The flow parameters are $k=0.9$ and $\sigma=4.0$. (b) The variation of the non-uniformity γ with gravity (decreasing Fr values) for $St=5$ and $St=25$. The flow parameters are $k=0.9$ and $\sigma=4.0$.

$$\frac{St}{Fr^2} > k \tag{16}$$

is satisfied, unconditionally stable *accumulation points* can exist in the flow-field, as opposed to the unstable or conditionally stable equilibrium points that are always present. Figure 17 displays several such cases of particle accumulation. In Fig. 17(a), the flow parameters $k=0.9$ and $\sigma=4.0$ establish only a single accumulation point for particles with $St=25$ and $Fr=5.25$, as $\sigma>\sigma_{cr}$, where σ_{cr} denotes the critical strain value πk. We have $St/Fr^2=0.907$, which is only slightly above the accumulation threshold of 0.9. Both from the pdf image and from the cross-stream distribution, one finds that a large number of particles have accumulated at the equilibrium point located on the symmetry line $z=0.5$ just below $y=0$. Here a small dark region in the pdf image corresponds to a large spike in the cross-stream distribution function.

In Fig. 17(b), $k=0.9$ and $\sigma=2$. Since the strain value is now subcritical, the flow parameters correspond to the case when triple equilibrium points can exist.[1] The terminal ve-

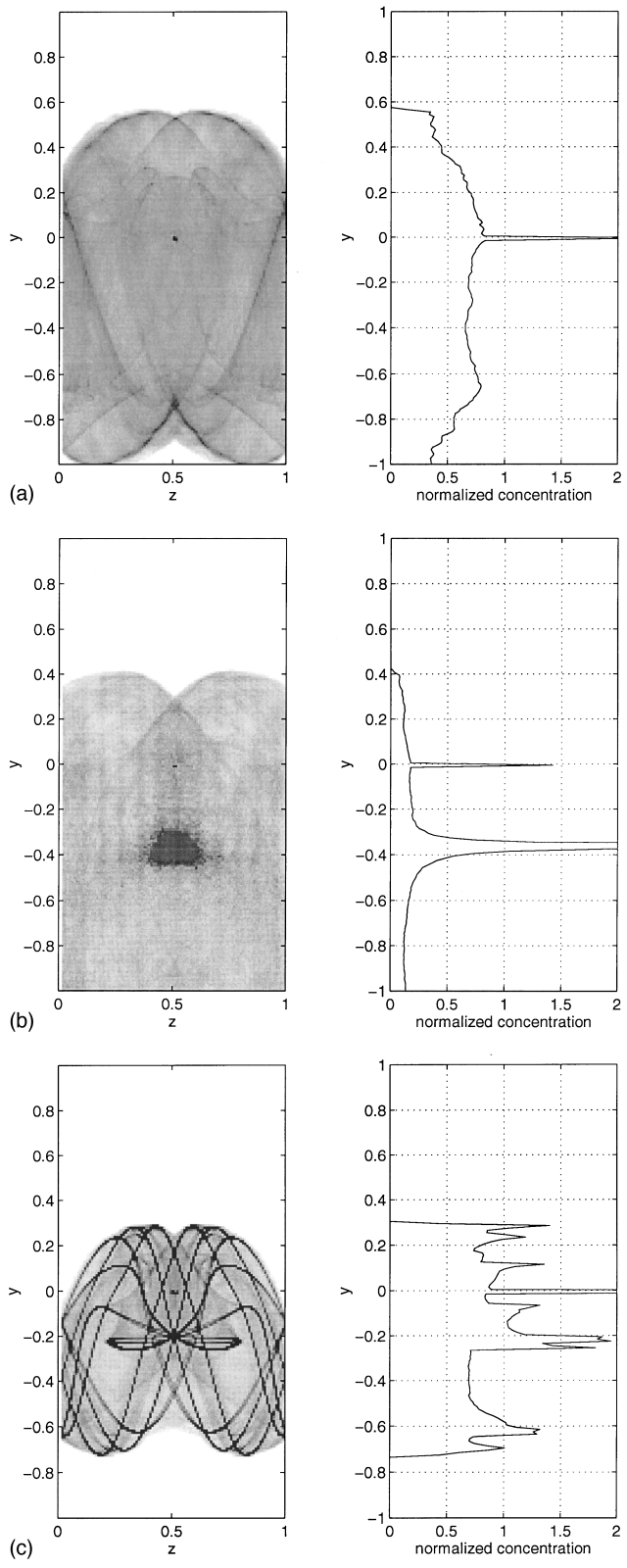

FIG. 17. Particle accumulation: probability distribution function and the corresponding cross-stream distribution profile. (a) $St=25, Fr=5.25$, $k=0.9$, and $\sigma=4.0$. Particle accumulation occurs at the unique stable equilibrium point. (b) $St=25, Fr=5.25, k=0.9$, and $\sigma=2.0$. Particle accumulation occurs at two stable equilibrium points. Significantly stronger accumulation can be observed at the lower equilibrium point. (c) $St=5, Fr=2.35, k=0.9$, and $\sigma=4.0$. Besides accumulation at the equilibrium point, strong collection of particles occurs along preferred trajectories.

locity is $St/Fr^2=0.907$, which is equal to the value for Fig. 17(a). Under these conditions, accumulation occurs at two of the three equilibrium points. The figure indicates that accumulation is considerably more pronounced at the lower one of the two points.

In Fig. 17(c), the flow parameters are $k=0.9$ and $\sigma=4$, corresponding again to the case when only one single accumulation point can exist. For the particle parameters $St=5$ and $Fr=2.35$, the terminal velocity $St/Fr^2=0.905$ is slightly above the accumulation limit. In this case, the lower $St=5$ value allows for the presence of preferred trajectories, along which many of the particles collect. This results in strong non-uniformities in the cross-stream distribution function, along with the accumulation spike.

In the accumulation cases presented above, the accumulation criterion (16) is exceeded only slightly. Consequently, many of the particles do not come to rest at the accumulation point, and instead continue their chaotic motion. Additional simulations conducted for terminal velocities that are 10% higher than the accumulation threshold show all particles accumulating. The condition (16) is therefore a necessary, but not sufficient, condition for accumulation of all particles in the flow field at the equilibrium point.

VI. CONCLUSIONS

The present computational investigation regarding the dynamics of heavy particles in the braid region of a three-dimensionally evolving mixing layer complements the mostly analytical results given in Part I.[1] There we addressed questions regarding the existence and linear stability of equilibrium points. However, when the interest focuses on questions regarding the dynamics of particles for which equilibrium points do not exist, or the size of the basin of attraction of those points, we have to rely on numerical simulations of the full nonlinear system. These issues are addressed here.

As was shown in Part I, only particles with fairly small values of St can be stably located at the centers of the stretched vortices. However, here we find that even for significantly larger values of St, particles remain trapped on closed loop trajectories around individual vortices. Only beyond a further critical value of St do these loops break open, so that particles can move to neighboring vortices. This threshold value of St depends both on the dimensionless strain rate σ, as well as on the dimensionless level of gravity expressed by the Froude number Fr. It is of interest to note that beyond this threshold particles can travel on one of two open trajectories, each of which does not reflect the symmetry of the underlying fluid velocity field. In other words, there exists a *spanwise transport mechanism* for the particles.

With increasing St, we observe a gradual transition to chaotic particle motion that involves symmetry breaking and period doubling bifurcations, as well as intermittency. Depending on the set of dimensionless governing parameters, this transition can occur below or above the threshold St value for the existence of open trajectories. The chaotic regime is characterized by random directional reversals of the particle motion, which frequently occur in the upwelling regions. Here gravity can roughly balance the viscous drag force, resulting in small particle velocities. For the chaotic particle motion regime, we investigated in some detail the two-dimensional probability distribution function as well as the averaged cross-stream distribution. Both of these show some non-uniformities, indicating the existence of regions and trajectories preferred by the particles. The degree of non-uniformity depends on the values of the governing parameters in a non-monotonic fashion. By means of a simplified one-dimensional model that could be solved analytically, we were able to derive scaling laws for the dependence of the cross-stream distribution width on the dimensionless strain rate σ and on St. These scaling laws agree well with the numerical data.

The influence of gravity leads to a breakup of the open trajectories into closed loops again, thereby disabling the spanwise particle transport. Furthermore, it shifts the particle concentration field in the direction of gravity, without affecting the cross-stream distribution width. Beyond a critical level of gravity, unconditionally stable accumulation points exist. If this critical level is only slightly exceeded, many but not all particles collect at these points. Only for even stronger gravity do all particles come to rest at the accumulation points.

It should be pointed out that the present study employs a simplified steady quasi-two-dimensional fluid velocity field, in order to gain detailed insight into the effects that stretched counterrotating vortices have on the dynamics of heavy particles. A real mixing layer is of course both three-dimensional and unsteady. As a result, the degree to which the mechanisms studied in isolation here will be observable in such unsteady three-dimensional flows, will depend, for example, on the relative time scales of the particle motion and the transient evolution of the fluid velocity field. Clearly, fully three-dimensional numerical simulations and experiments are needed in order to investigate these issues. However, the present observations and results can guide the analysis and interpretation of the data obtained from such future investigations.

ACKNOWLEDGMENTS

The authors gratefully acknowledge support by the National Science Foundation under Grant No. CTS-9196004, and by the Electric Power Research Institute. Computing resources were provided by the San Diego Supercomputer Center.

[1] B. Marcu and E. Meiburg, "The effect of the streamwise braid vortices on the particle dispersion in a plane mixing layer. I. Equilibrium points and their stability," Phys. Fluids **8**, 715 (1996).
[2] L. P. Bernal and A. Roshko, "Streamwise vortex structures in plane mixing layers," J. Fluid Mech. **170**, 499 (1986).
[3] J. C. Lasheras and H. Choi, "Three-dimensional instability of a plane, free shear layer: An experimental study of the formation and evolution of streamwise vortics," J. Fluid Mech. **189**, 53 (1988).
[4] J. H. Bell and R. D. Mehta, "Measurements of the streamwise vortical structures in a plane mixing layer," J. Fluid Mech. **239**, 213 (1992).
[5] W. T. Ashurst and E. Meiburg, "Three dimensional shear layers via vortex dynamics," J. Fluid Mech. **189**, 87 (1988).
[6] S. J. Lin and G. M. Corcos, "The mixing layer: Deterministic models of a turbulent flow. Part 3. The effect of plane strain on the dynamics of streamwise vortices," J. Fluid Mech. **141**, 139 (1984).
[7] C. T. Crowe, R. A. Gore, and T. R. Troutt, "Particle dispersion by coherent

structures in free shear flows,'' Part. Sci. Technol. **3**, 149 (1985).
[8]B. J. Lazaro and J. C. Lasheras, ''Particle dispersion in a turbulent, plane, free shear layer,'' Phys. Fluids A **1**, 1035 (1989).
[9]B. J. Lazaro and J. C. Lasheras, ''Particle dispersion in the developing free shear layer. Part I: Unforced flow,'' J. Fluid Mech. **235**, 143 (1992).
[10]B. J. Lazaro and J. C. Lasheras, ''Particle dispersion in the developing free shear layer. Part 2: Forced flow,'' J. Fluid Mech. **235**, 179 (1992).
[11]J. E. Martin and E. Meiburg, ''The accumulation and dispersion of heavy particles in forced two-dimensional mixing layers. Part I: The fundamental and subharmonic cases,'' Phys. Fluids **6**, 1116 (1994).
[12]N. Raju and E. Meiburg, ''The accumulation and dispersion of heavy particles in forced two-dimensional mixing layers. II. The effect of gravity,'' Phys. Fluids (in press).
[13]M. R. Maxey and J. J. Riley, ''Equation of motion for a small rigid sphere in a nonuniform flow,'' Phys. Fluids **26**, 883 (1983).
[14]A. M. Gañan Calvo and J. C. Lasheras, ''The dynamics and mixing of small spherical particles in a plane, free shear layer,'' Phys. Fluids A **3**, 1207 (1991).
[15]K.-K. Tio, A. M. Gañan Calvo, and J. C. Lasheras, ''The dynamics of small, heavy, rigid spherical particles in a periodic Stuart vortex flow,'' Phys. Fluids A **5**, 1679 (1993).
[16]G. M. Corcos and F. S. Sherman, ''The mixing layer: Determination models of a turbulent flow. Part I. Introduction and the two-dimensional flow,'' J. Fluid Mechanics **139**, 29 (1984).
[17]J. M. Burgers, ''A mathematical model illustrating the theory of turbulence,'' Adv. Appl. Mech. **1**, 171 (1948).
[18]B. Marcu, E. Meiburg, and P. K. Newton, ''Dynamics of heavy particles in a Burgers vortex,'' Phys. Fluids **7**, 400 (1995).
[19]M. J. Feigenbaum, *Nonlinear Dynamics and Turbulence: Universal Behavior of Non-linear Systems*, edited by G. I. Barenblatt, G. Ioss, and D. D. Joseph (Pitman, New York, 1983).
[20]Y. Pomeau, *Nonlinear Dynamics and Turbulence: The Intermittent Transition to Turbulence* edited by G. I. Barenblatt, G. Ioss, and D. D. Joseph, (Pitman, New York, 1983).
[21]J. C. Neu, ''The dynamics of stretched vortices,'' J. Fluid Mech. **143**, 253 (1984).